Dust accumulation biases in PIRATA shortwave radiation records

Gregory R. Foltz[1], Amato T. Evan[2], H. Paul Freitag[3], Sonya Brown[3,4], and Michael J. McPhaden[3]

[1]NOAA/Atlantic Oceanographic and Meteorological Laboratory, Miami, FL
[2]Scripps Institution of Oceanography, University of California at San Diego, La Jolla, CA
[3]NOAA/Pacific Marine Environmental Laboratory, Seattle, WA
[4]Univ. Washington/JISAO, Seattle, WA

21 February 2013

Revised for *J. Atmos. Ocean. Tech.*

Corresponding author: gregory.foltz@noaa.gov

Abstract

Long-term and direct measurements of surface shortwave radiation (SWR) have been recorded by the Prediction and Research moored Array in the Tropical Atlantic (PIRATA) since 1997. Previous studies have shown that African dust, transported westward from the Sahara and Sahel regions, can accumulate on mooring SWR sensors in the high-dust region of the North Atlantic (8°N–25°N, 20°W–50°W), potentially leading to significant negative SWR biases. Here dust-accumulation biases are quantified for each PIRATA mooring using direct measurements from the moorings, combined with satellite and reanalysis data sets and statistical models. The SWR records from five locations in the high-dust region (8°N, 12°N, and 15°N along 38°W; 12°N and 21°N along 23°W) are found to contain monthly mean accumulation biases as large as -200 W m^{-2} and record-length mean biases on the order of -10 W m^{-2}. The other 12 moorings, located mainly between 10°S–4°N, are in regions of lower atmospheric dust concentration and do not show statistically significant biases. Seasonal to interannual variability of the accumulation bias are found at all locations in the high-dust region. The moorings along 38°W also show decreasing trends in the bias magnitude since 1998 that are possibly related to a corresponding negative trend in atmospheric dust concentration. The dust-accumulation biases described here will be useful for interpreting SWR data from PIRATA moorings in the high-dust region. The biases are also potentially useful for quantifying dust deposition rates in the tropical North Atlantic, which at present are poorly constrained by satellite data and numerical models.

1 Introduction

The Prediction and Research moored Array in the Tropical Atlantic (PIRATA) consists of 17 long-term Autonomous Temperature Line Acquisition System (ATLAS) buoys equipped with sensors to measure near-surface meteorological and subsurface oceanic parameters (Bourlès et al. 2008; Fig. 1). The moorings are a unique component of the tropical Atlantic observing system, providing long time series (15 years and growing) at a high temporal resolution (1–10 min averages). In contrast to moving platforms such as drifting buoys and floats, PIRATA moorings remain fixed, providing colocated air-sea measurements that are valuable for studying ocean-atmosphere interaction on diurnal to decadal timescales (e.g., Bourlès et al. 2008 and references therein).

The near-surface atmospheric measurements from PIRATA are in general of significantly higher quality than those inferred from satellites and simulated by models, making the PIRATA moorings a valuable tool for identifying biases in satellite- and reanalysis-based estimates of surface turbulent heat fluxes (Sun et al. 2003, Kumar et al. 2012), rainfall (Serra and McPhaden 2003), and shortwave radiation (SWR; Pinker et al. 2009, Kumar et al. 2012). Nevertheless, the meteorological sensors on the moorings are exposed to elements such as sea-spray, natural and anthropogenic aerosols, and severe weather during each year-long deployment. The sensors therefore occasionally develop time-dependent drifts or biases. In most cases, systematic errors are identified from the near-real-time data streams or from the internally stored data after a mooring is recovered (Freitag et al. 1994). The suspicious data are then either flagged, or a correction is applied based on the results of post-deployment calibration. Similar quality-control procedures are used on data from ATLAS moorings in the tropical Pacific and Indian Oceans (McPhaden et al. 1998, 2009).

One unique aspect of the tropical Atlantic that complicates quality-control procedures for PIRATA data is the presence of large quantities of African dust in the atmosphere of the tropical North Atlantic (Prospero and Carlson 1972, Kaufman et al. 2005; Fig. 1). Most of the dust originates from the Sahel and Sahara regions of Africa and is blown westward over the ocean by the surface and mid-level easterly winds (Prospero et al. 2002, Moulin and Chiapello 2004, Kaufman et al. 2005). The highest dust aerosol optical depth (τ_{dust}) is found between 8°N–20°N (Fig. 1), north of the heaviest band of precipitation associated with the intertropical convergence zone (ITCZ).

About 60% of the ∼240 Tg of dust that are transported westward from Africa falls to the tropical and subtropical North Atlantic Ocean (Ginoux et al. 2001, Gao et al. 2001, Kaufman et al. 2005). Most deposition occurs during boreal summer and fall, when dust export from Africa is highest. Northward of about 10°N, τ_{dust} shows a pronounced peak in boreal summer. The peak shifts from summer to spring and decreases in magnitude southward from 10°N to the equator (Kaufman et al. 2005). It is therefore not surprising that the meteorological sensors on PIRATA moorings in the tropical North Atlantic accumulate a substantial layer of dust during year-long deployments (Medovaya et al. 2002, Foltz and McPhaden 2005). Of the instruments on the PIRATA moorings, accumulated dust is most likely to interfere with the SWR radiometer, an upward-facing glass dome that is fully exposed to falling dust. Indeed, dust buildup has been observed on several PIRATA moorings in the tropical North Atlantic during servicing cruises (Freitag and Brown, manuscript in preparation).

The potential for dust buildup to interfere with SWR measurements on open-ocean moorings was first acknowledged by Moyer and Weller (1997). They found traces of red sand on the instrumentation of the Southeast Subduction Experiment buoy at 18°N, 22°W and suggested that its presence on the radiometer might have reduced the measured insolation. Waliser et al. (1999) further showed that daytime clear-sky SWR meaurements from the Subduction buoy were biased low by about 70 W m^{-2} relative to those estimated from a radiative transfer model. They concluded that the most likely cause of the bias was accumulation of African dust on the radiometer. However, they noted that post-deployment calibrations performed with and without the dust coating on the sensor differed by only 1%, or about 5 W m^{-2}, leading them to suspect that some of the dust may have fallen off the sensor either while in the field or during transit to the post-deployment calibration site. Medovaya et al. (2002) compared clear-sky measurements of SWR from several open-ocean moorings to estimates from a model. They found significant mean differences at several locations, including the Southeast Subduction buoy, that they attributed to a combination of radiometer tilt (due to ocean currents or deployment technique), clear-sky model biases, and aerosol buildup on the radiometer. Foltz and McPhaden (2005) found discontinous upward jumps in SWR of $\sim$50 W m^{-2} from the 15°N, 38°W PIRATA buoy immediately following servicing cruises that they attributed to dust buildup on the radiometer.

Laboratory comparisons between dusty sensors recovered from PIRATA moorings in the tropical North Atlantic and a newly calibrated sensor showed that the output from the dusty sensors was biased low by up to 14% (Freitag and Brown, manuscript in preparation). The comparisons also showed that for clear-sky conditions, the magnitude of the bias can depend strongly on the solar zenith angle, whereas under cloudy conditions the bias is more constant throughout the day. The difference likely results from an uneven distribution of dust on the radiometer dome.

Previous strategies for dealing with dust buildup on mooring sensors include discarding all SWR data that are contaminated (Waliser et al. 1999), using the data without any correction (Pinker et al. 2009, Kumar et al. 2012), or applying a linear time-dependent correction backward in time from radiometer swap dates (Foltz and McPhaden 2005). Each approach has distinct disadvantages. Discarding all data contaminated by dust buildup would eliminate several years' worth of SWR records from each PIRATA mooring in the tropical North Atlantic (8°N–21°N). On the other hand, there is evidence of significant time-dependent negative biases in the Southeast Subduction and PIRATA SWR time series that should be accounted for prior to their use in scientific analyses. The method used by Foltz and McPhaden (2005) worked reasonably well for analyzing intraseasonal (30–70 day period) variability since the dust-accumulation bias is expected to increase in magnitude gradually over several months. The same method was used to study an anomalous event during a single year, though in this case SWR measurements from another mooring without significant dust buildup were used for validation of the corrected SWR time series (Foltz and McPhaden 2006). The linear correction method does not take into account rinsing of the radiometer dome by rainfall, and it is unknown how much uncertainty is involved with calculating the dust-accumulation bias from pre- and post-swap SWR values. Furthermore, it is unclear whether the SWR attenuation caused by dust buildup increases linearly in time or is a more complex function of τ_{dust} and possibly other parameters.

In this study a more rigorous technique is developed to calculate dust-accumulation biases in PIRATA SWR records. The corrected time series are found to be more consistent with observed cloud cover in the tropical Atlantic over the past 13 years and agree better with satellite-derived SWR estimates over the same time period.

2 Data

The primary data set consists of daily-averaged SWR measurements from 17 PIRATA moorings (Fig. 1). The moorings have acquired a combined total of 120 years of SWR data since 1997 (Fig. 2) and sample a wide variety of SWR regimes, including the stratus deck of the southeastern tropical Atlantic, the intertropical convergence zone (ITCZ), and the region of high τ_{dust} to the north of the ITCZ. Several other satellite and reanalysis data sets are used in conjunction with PIRATA data to calculate dust-accumulation biases.

2.1 PIRATA

Each PIRATA buoy is equipped with an Eppley pyranometer that measures down-welling SWR in the range of 0.285 to 2.8 μm. The sensor is mounted at a height of 3.5 m, and values are recorded as 2-min means. Here we use the daily-averaged data through March 2011. The sensors are deployed for about one year on average. During each servicing cruise, the SWR sensor is recovered with the mooring, and a new sensor is deployed. The earliest time series begin in 1997, and the most recent time series start in 2007. Because of gaps in most of the records, the usable portion of each time series ranges from 3 to 13 years in length (Figs. 1, 2).

Uncertainties in SWR measurements from the moorings are estimated to be $\pm$ 3% based on pre- and post-deployment calibration (Freitag and Brown, manuscript in preparation). In all cases, post-deployment calibrations were performed with clean sensors (i.e., rinsed of any sea salt or aerosol residue). These instrumental errors are likely a lower bound on the uncertainties of the SWR measurements in the field, which also include errors due to buoy tilt and salt/aerosol buildup on the sensor. Errors due to buoy tilt are difficult to quantify (MacWhorter and Weller 1991), but are likely to be significant only at locations with strong mean currents (i.e., in the strong westward flow along the equator and eastward flow between 4°N–8°N in the tropical Atlantic). Buoy tilt biases are therefore expected to be largest at the 8°N, 38°W mooring location, where maximum monthly mean current speed is $\sim$40 cm s^{-1}, based on Ocean Surface Current Analysis-Realtime (OSCAR) data averaged during 1992–2011 (Bonjean and Lagerloef 2002). Tilt biases are not expected to be significant in the 12°N–21°N latitude band, where monthly mean current speeds are <20 cm s^{-1}. None of the PIRATA SWR time series that is used in this study has been corrected for buoy tilt, nor for salt/aerosol (including dust) buildup on the sensor.

In addition to SWR, we use daily-averaged rainfall from each PIRATA mooring. Rainfall, measured at a height of 3.5 m by an R. M. Young capacitive rain gauge, is used to identify when the SWR sensor would be rinsed of dust.

2.2 Satellite and reanalysis products

Several satellite and reanalysis data sets aid in quantifying the buoy dust-accumulation biases. Because direct measurements of dust deposition are not available at the PIRATA moorings, we rely on satellite-based estimates of aerosol optical thickness (AOT). Daily-averaged AOT at 550 nm is available from the Moderate Resolution Imaging Spectroradiometer (MODIS) onboard the *Aqua* and *Terra* satellites at a horizontal resolution of 1° (Remer et al. 2005). Data from *Terra* are used for February 2000 through July 2002 and from *Aqua* during July 2002 through March 2011. Daily MODIS fine mode fraction (FMF), proportional to the size of scattering aerosol, is used with MODIS AOT and surface wind speed (described later) to calculate dust aerosol optical thickness (τ_{dust}). We also use daily MODIS primary cloud fraction and cloud optical thickness (τ_{cloud}) to determine the impact of clouds on SWR measured by the moorings.

Since many of the PIRATA records begin before the launch of MODIS in 2000, monthly mean AOT at 670 nm from the Advanced Very High Resolution Radiometer (AVHRR) Pathfinder Extended dataset (PATMOS-x) is used to extend the MODIS record back in time from February 2000 to the start of the PIRATA SWR record. The PATMOS-x data are available during 1982–2011 on a 0.5° grid (Ignatov and Stowe 2002, Evan et al. 2006). The MODIS cloud fraction is extended backward using International Satellite Cloud Climatology Project (ISCCP) data for the period 1998–2000 on a 2.5° grid (Rossow and Schiffer 1991). Monthly mean climatological MODIS FMF and τ_{cloud} are used for the 1998–2000 period since reliable replacements are not available.

Daily averaged SWR is obtained from the ISCCP Flux Dataset (ISCCP-FD) for the period 1998–2009 on a 2.5° grid (Zhang et al. 2004). This product uses ISCCP cloud retrievals and atmospheric reanalysis products as input to a radiative transfer model to calculate surface and top of the atmosphere shortwave and longwave radiation. Daily surface clear-sky solar radiation is available from the NCEP/NCAR reanalysis (Kalnay et al. 1996) during 1948–2011 on a 2° grid and from the Modern Era Retrospective analysis for Research and Applications (MERRA; Rienecker et al. 2011) during 1979–2011 on a $\frac{2}{3}^{\circ}$-lon$\times\frac{1}{2}^{\circ}$-lat grid. Here we use the data for the period 1998–2011. The NCEP/NCAR reanalysis clear-sky SWR product does not include dust aerosols explicitly, whereas the MERRA product includes the seasonal cycle of dust aerosol radiative forcing. The NCEP/NCAR and MERRA reanalyses also use different input data and different radiative transfer models to calculate clear-sky radiation.

The differences in clear-sky radiation between the data sets therefore reflect differences between two independent methods, each with its own strengths and weaknesses. Precipitation rate from the Tropical Rainfall Measuring Mission (TRMM) precipitation radar are available during 1998–2011 on a 0.5° grid. Here we use the hourly gridded product (3G68 from NASA/GSFC) averaged to a daily resolution. These data are used to fill gaps in the PIRATA precipitation records.

3 Methodology

In this section we first describe the methods used to calculate τ_{dust} and an index representing the magnitude of the dust-accumulation bias at a given mooring location. We then describe the methodology used to calculate time series of the dust-accumulation bias.

3.1 τ_{dust} and dust-accumulation index

We calculate τ_{dust} following the methodology of Kaufman et al. (2005):

$$\tau_{dust} = \frac{AOT(0.9 - FMF) - 0.6\tau_{marine}}{0.4} \tag{1}$$

$$\tau_{marine} = 0.007W + 0.02 \tag{2}$$

Here τ_{marine} is the optical depth of particles such as sea salt and sulfates, which are produced from the oxidation of ocean-produced organic material, and W is monthly climatological NCEP/NCAR reanalysis surface wind speed for the period 1998–2010, interpolated to a daily resolution.

To determine which PIRATA locations exhibit significant dust-accumulation biases, we define a dust-accumulation bias index, which represents the maximum bias averaged over all sensor deployments and at a given location. Two different methods of calculating the index are described: the "rain-free" and "swap" methods.

For the rain-free method, we start by defining a "rain-free" segment of a full SWR time series as one which falls completely between sensor swap dates and in which rainfall on every day of the segment is less than 5 mm. This ensures that, in principle, dust is continually accumulating on the sensor since it is not being rinsed by rain. The bias for each rain-free segment with a length >75 days is then calculated as the difference between the buoy SWR anomaly (with respect to ISCCP-FD daily mean seasonal cycle) averaged over the first 30 days of the segment and the buoy SWR anomaly averaged over the last 30 days of the segment. The monthly mean seasonal cycle of ISCCP-FD SWR is subtracted from the buoy SWR before computing the bias to account for the strong seasonal cycle of SWR at most locations. The individual biases calculated from each rain-free segment at a given PIRATA location are then averaged, giving a single-valued dust accumulation bias index. Statistical significance of each index is assessed using a Student's t-test with $p = 0.05$. Indices are not computed for locations with less than three rain-free segments of at least 75 days in length. All locations satisfy this criterion except 4°N, 38°W and 4°N, 23°W, where annual mean rainfall is highest.

To calculate the dust-accumulation index using the "swap" method, the mean of the buoy SWR anomaly (with respect to the daily mean ISCCP-FD SWR seasonal cycle) during the 30-day period immediately before a sensor swap is subtracted from the mean buoy SWR anomaly during the 30 days immediately after a sensor swap. Because of gaps in the buoy SWR time series at the end of some deployments, there are fewer swap bias estimates than rain-free estimates. The swap bias estimates are also more sensitive to anomalies in SWR related to changes in cloudiness, since there is sometimes significant rainfall immediately before or after a sensor swap. For this reason, we use only the highest 15 daily SWR values from each 30-day pre- and post-swap period for calculating each mean. This decreases the likelihood of including cloudy days in the means, which would bias the calculation. Note that the "rain-free" and "swap" bias indices are defined as positive when there is an attenuation of SWR due to accumulated dust (i.e., a negative bias in the SWR time series).

For validation of the "swap" biases we have also calculated the SWR bias directly from five dusty sensors that were recovered from the 15°N, 12°N, and 8°N PIRATA moorings along 38°W during April 2002 and July 2003 (Freitag and Brown, manuscript in preparation). The output from each recovered sensor was compared to a clean, calibrated sensor during a period of 28 days. The sensors were placed in direct sunlight outside the Pacific Marine Environmental Laboratory in Seattle and experienced both sunny and overcast conditions. The radiometers were then cleaned and calibrated either by the manufacturer (The Eppley Laboratory, Inc.) or the National Renewable Energy Laboratory in order to quantify sensor drift unrelated to dust accumulation. The dust-accumulation bias for each sensor was calculated as

$$B_{lab} = S_{clim}(P_{tot} - P_{drift}) \tag{3}$$

where S_{clim} is the 1998–2011 climatological mean ISCCP-FD SWR on the calendar day of the sensor recovery, P_{tot} is the mean bias from the laboratory comparison with the dusty sensor, and P_{drift} is the mean bias of the clean sensor after removal of all dust. The P_{tot} and P_{drift} biases are expressed as a percentage of the total incoming solar radiation and represent averages over the full 28 days of the experiment (day and night). For consistency, the values of B_{lab} are not included in the calculation of the dust-accumulation index nor in the time-dependent bias correction methodologies described next, but are shown and described in section 4.

The methods described above give a single-valued, time-independent, dust-accumulation bias at a given mooring location. In order to quantify the time-dependence of the bias, three independent methods were developed: "rain-free,", "swap," and "clear-sky." These methods are described in the remainder of this section.

3.2 Rain-free

To calculate dust-accumulation biases using the rain-free method, first the monthly mean seasonal cycle of ISCCP-FD SWR at a given PIRATA location is interpolated to a daily resolution and subtracted from the daily PIRATA SWR time series. This gives a daily time series of PIRATA SWR anomalies for the length of the PIRATA record. As in the rain-free index calculation, the time-dependent bias calculation is only performed on segments of the time series that are between sensor swaps and that have no significant rainfall.

A rainfall criterion of 5 mm day^{-1} was used to define rain-free segments for the index calculation. This criterion was chosen because we were interested in finding the maximum bias before any rinsing of the sensor had occurred. For the time-dependent bias calculation in this section we use a criterion of 50 mm accumulated over a period of 30 days. This choice allows for partial rinsing and is based on examination of the rainfall and SWR records from the moorings along 38°W. The results are similar for other reasonable choices of the rainfall criterion since at most locations there is a well-defined start to the rainy season.

The buoy SWR anomalies in each rain-free segment are the result of forcing from several sources: (1) anomalies of clouds, water vapor, and aerosols suspended in the atmosphere, (2) dust build-up on the buoy SWR sensor, and (3) biases in the ISCCP-FD SWR climatology caused, for example, by changes in satellite coverage and limited measurements of the vertical profiles of suspended aerosols. Since the goal is to quantify the SWR signal associated with (2), ideally (1) and (3) should be completely removed from the buoy SWR anomaly time series, giving the dust accumulation bias as a residual. However, it is difficult to remove the SWR variability due to clouds, water vapor, and aerosols, and it is also challenging to quantify biases in ISCCP-FD SWR since the only in situ measurements are from PIRATA, and they are biased by dust buildup. An alternative technique is to model the dust accumulation bias as a function of one or more time-dependent variables. Developing a model that describes time-dependent SWR biases from dust buildup would require knowledge of the rate of dust accumulation on the sensor as a function of meteorological conditions and τ_{dust}. These relationships cannot be determined confidently with the available data. We therefore use a hybrid technique, which is described below.

First, anomalies of SWR due to clouds and suspended dust are removed from the daily PIRATA SWR anomaly time series. Based on time series of clear-sky SWR from NCEP and MERRA reanalyses, we have found that nonseasonal variability of water vapor-induced SWR is much weaker compared to the SWR signals from clouds and suspended dust and therefore do not remove the water vapor signal. Since the removal of the cloud- and dust-induced signals is not perfect and the remaining cloud- and dust-free signal may be contaminated by biases in ISCCP-FD SWR, we fit a curve to each rain-free segment of the cloud- and dust-free SWR anomaly time series. The curve is based on the observed dependence of buoy SWR anomalies on the time-integral of

τ_{dust}. In the rest of this subsection the details of this method are described, beginning with the removal of the cloud and τ_{dust} signals, followed by the curve-fitting procedure.

Attenuation of SWR by clouds (SWR_{cloud}) is assumed to be proportional to one minus the direct transmittance of light through the cloud layer, times the total cloud fraction:

$$SWR_{cloud} \propto f(1 - e^{-\tau_{cloud}}) \tag{4}$$

Here f is total cloud fraction and τ_{cloud} is cloud optical depth, both from daily mean MODIS data and with the corresponding mean seasonal cycle removed. For the period before February 2000 when MODIS data are not available we use ISCCP f and the monthly mean climatology of MODIS τ_{cloud} since we have found that nonseasonal variability of τ_{cloud} is small compared to that of f. In order to avoid contamination by dust-accumulation biases in the buoy SWR data, the SWR anomaly time series is filtered using a high-pass Lanczos filter with a cut-off period of 120 days and 100 coefficients. A third-order polynomial is then fit to the daily high-pass filtered SWR anomalies, from a given PIRATA mooring, as a function of the righthand side of (4). The results from three locations along 38°W are shown in Fig. 3. The model works reasonably well northward of 8°N, but has difficulty predicting cloud forcing anomalies for large positive anomalies of $f(1-exp(-\tau_{cloud}))$ at 8°N, 38°W. Nonlinearity of the fits in Fig. 3 is caused by the diffuse transmittance of light, which is difficult to quantify and is not included in (4).

Attenuation of SWR by suspended dust (SWR$_{dust}$) is calculated as a function of calendar month, latitude, and τ_{dust}, at each mooring location, following Evan and Mukhopadhyay (2010). On average, SWR$_{dust}$ is about 70 W m^{-2} per unit of τ_{dust} in the tropical North Atlantic, consistent with other studies (e.g., Zhu et al. 2007). Anomalies of SWR$_{dust}$ from the seasonal cycle are generally weaker than anomalies of SWR$_{cloud}$, which is expected since clouds are optically much thicker than dust plumes. At the high-dust PIRATA locations the daily, record-length, standard deviation of SWR$_{cloud}$ anomalies ranges from 22–31 W m^{-2}, whereas for anomalies of SWR$_{dust}$ the range is 14–15 W m^{-2}. For 180-day low-passed time series, the anomaly standard deviation of SWR$_{cloud}$ ranges from 6–7 W m^{-2} and SWR$_{dust}$ ranges from 3–4 W m^{-2}. The low-passed values are significantly lower than the accumulation bias indices (described in the next section), indicating that a large portion of the anomalous SWR variability at the high-dust locations results from dust buildup on the sensors.

After removing SWR anomalies due to clouds and suspended dust from the PIRATA SWR anomaly time series, the remaining signal (SWR$_{resid}$) contains variability associated with dust buildup on the sensor and, ideally, only a much smaller signal from anomalies in water vapor and trace gases, which have not been removed. In reality, the combination of clouds and suspended dust explains only about 30% of the nonseasonal SWR variability at the high-dust locations. It is also possible that there are significant biases in the ISCCP-FD SWR climatology. We therefore estimate the measured dust-accumulation SWR bias by fitting a curve to each rain-free segment of the PIRATA SWR$_{resid}$ time series of the form

$$SWR_{accum}(t) = (c_1 - c_2 e^{-c_3 \tau_{dust}^{int}(t)}) \tag{5}$$

$$\tau_{dust}^{int}(t) = \int_{t_0}^{t_{end}} \tau_{dust} dt \tag{6}$$

Here $\tau_{dust}^{int}(t)$ is the time-integral of τ_{dust} between t_0, the first day of a given rain-free segment, and t_{end}, the last day of the rain-free segment. In (5), we set $c_1 = 200$ W m^{-2}.

Results are not sensitive to the choice of c_1 as long as it is greater than the maximum observed dust-accumulation bias. The constants c_2 and c_3 are determined through an iterative procedure that fits the righthand side of (5) to each rain-free SWR$_{resid}$ time series at a given PIRATA location. The parameterization in (5) assumes that the dust-accumulation bias is proportional to the time-integral of τ_{dust} under rain-free conditions and not τ_{dust} itself. This assumption is based on the observation that most dust-accumulation biases increase in magnitude with time, until rainfall commences or there is a sensor swap. Further justification of (5) is shown in Fig. 4. There is a clear negative bias in buoy SWR that increases in magnitude as τ_{dust}^{int} increases (Fig. 4a). In contrast, there is not a strong relationship between buoy SWR anomalies and τ_{dust} (Fig. 4b). On average, the relationship between SWR$_{resid}$ and τ_{dust}^{int} is nearly linear, possibly because the amount of dust that sticks to the sensor, for a given deposition rate, decreases as the amount of dust on the sensor increases. Note that in (5), positive values of SWR$_{accum}$ indicate a reduction in SWR recorded by the buoy sensor, for consistency with the sign of the dust-accumulation bias indices described earlier in this section.

The purpose of fitting the righthand side of (5) to each SWR$_{resid}$ segment is to reduce the chance that seasonally-varying ISCCP-FD SWR biases or unresolved natural SWR variability (i.e., due to cloudiness or τ_{dust} anomalies) are interpreted as a dust-accumulation bias. For example, (5) ensures that a large negative SWR anomaly in SWR$_{resid}$ that is actually due to increased cloud cover will be significantly reduced in magnitude if there is not a corresponding increase in τ_{dust}^{int}. The application of (5) to each rain-free segment also acts as a low-pass filter, eliminating most of the high-frequency SWR variability that is unrelated to more slowly-evolving dust buildup. In order to eliminate mean biases that may be present in the ISCCP-FD SWR climatology, the value of SWR_{accum} at the beginning of a given rain-free segment is subtracted from the $\mathrm{SWR}_{accum}(t)$ time series.

3.3 Swap

The rain-free method for computing time-dependent dust-accumulation biases relies on the ISCCP-FD SWR climatology, which may contain significant seasonally-dependent biases. We therefore consider an alternative method that is based on the difference between the buoy SWR anomaly before and after a sensor swap. The procedure is as follows. First, the swap bias (ΔSWR) at the end of each deployment is calculated as described earlier in this section. Each ΔSWR is then extended back in time either until the significant rain threshold is satisfied or until the previous sensor swap. In either case, it is assumed that the dust-accumulation bias is zero at the beginning of the time segment. The magnitude of the time-dependent swap bias (SWR_{swap}) is assumed to increase from zero at the beginning of the time segment to ΔSWR at the end. The rate of decrease of SWR_{swap} depends on the time-integral of τ_{dust} (equations 5, 6).

The advantage of this method is that the dust accumulation bias at the end of a given deployment is calculated by comparing SWR values from a dusty sensor to those from a sensor that is known to be clean. The sensor swap takes only one day to complete, and ΔSWR is calculated as the difference between the SWR anomaly averaged over the 30-day period after a sensor swap and the SWR anomaly averaged over the 30-day period prior to the sensor swap. We have found that the results of the "swap" method are not strongly sensitive to the choice of the time periods before and after the sensor swap that are used to calculate ΔSWR.

3.4 Clear-sky

Neither the "rain-free" nor the "swap" methods calculates the dust-accumulation bias during periods of significant rainfall. Instead, it is assumed that the bias goes to zero after a certain rainfall threshold is reached. This is a disadvantage of these techniques, since a complete rinsing of the sensor can occur over a period of several months at some locations. In addition, for the rain-free method, calculation of the SWR forcing due to clouds is complicated by a mismatch in spatial scales between the mooring and the satellite footprint, and uncertainties in the statistical and radiative transfer models. In this section a third method is described that gives a continuous daily time series of the dust-accumulation bias and does not rely on satellite data for cloud removal.

On a given cloud-free day, the difference between the buoy SWR and the modeled clear-sky SWR is, in principle, the dust-accumulation bias. The challenge in implementing the "clear-sky" method is therefore the identification of cloud-free days in the buoy record and the use of an appropriate clear-sky model. To identify cloud-free days in the PIRATA SWR time series, a centered 30-day running-maximum filter is applied. This gives a daily time series of the maximum daily-averaged SWR value in a window of ± 15 days under the assumption that there is at least one cloud-free day during that interval. Examination of daily MODIS cloud fraction at each high-dust location revealed that during a given 30-day period there are, on average, 2–3 days with cloud coverage of $<5\%$. Cloud coverage is most persistent at 8°N, 38°W, where there are 913 thirty-day segments between July 2002 and April 2011 without a day in which cloud cover is $<5\%$. The magnitude of the dust-accumulation biases may therefore be overestimated when calculated using the clear-sky method, especially at 8°N, 38°W.

The clear-sky SWR estimates based on the buoy time series ($\mathrm{SWR}_{cs-biased}$) contain the dust accumulation bias as well as variability in clear-sky SWR due to changes in the solar zenith angle and changes in water vapor and aerosols in the atmosphere. The dust bias signal is therefore estimated as the residual between $\mathrm{SWR}_{cs-biased}$ and an estimate of the "true" clear-sky SWR (SWR_{cs}). Three independent estimates of SWR_{cs} are considered: one based on the buoy SWR time series and two from atmospheric reanalyses (NCEP and MERRA).

To calculate the "true" clear-sky SWR (SWR_{cs}) from the buoy time series, first the biased clear-sky time series ($\mathrm{SWR}_{cs-biased}$) is calculated using the method described above. This time series includes biases due to dust buildup. From all years, the maximum $\mathrm{SWR}_{cs-biased}$ value is chosen for each calendar day in an attempt to create a daily clear-sky SWR climatology that is not contaminated by dust-accumulation biases. This method is expected to work well when the SWR sensors are rinsed or swapped at different times of the year since there is likely to be a different period during each year with very little dust buildup. The method will also perform better at locations with long records since there are potentially more data available that are not strongly contaminated by dust buildup. This is verified by an experiment in which a certain number of years of data (less than the number of years in the time series) were chosen at random from the full buoy time series before calculating SWR_{cs} (Fig. 5). In general, about seven years of data are needed to reduce errors in buoy-derived SWR_{cs} below 5 W m^{-2} at the high-dust locations. We therefore expect a high degree of uncertainty associated with this method at the locations along 23°W, where record lengths are less than 4 years.

The SWR_{cs} estimates from the NCEP and MERRA reanalyses have similar seasonal cycles at each PIRATA location, but significant mean offsets (Fig. 5a). As expected, the annual mean NCEP SWR_{cs} is significantly larger than the annual mean of MERRA SWR_{cs} since NCEP SWR_{cs} does not include radiative forcing from dust aerosols. The offsets are corrected by subtracting the record-length mean difference between the reanalysis and buoy SWR_{cs} averaged at all low-dust PIRATA locations. Similarly, in order to account for possible contamination from cloudiness in $SWR_{cs-biased}$, the mean difference between $SWR_{cs-biased}$ and buoy SWR_{cs}, averaged at all low-dust locations, is subtracted from $SWR_{cs-biased}$. It is assumed that the resultant estimates of SWR_{cs} from MERRA and the buoy include the mean seasonal cycle of SWR-forcing from τ_{dust}, but do not account for SWR-forcing from anomalies of τ_{dust}, which are present in $SWR_{cs-biased}$. Before calculating the clear-sky bias using the MERRA and buoy SWR_{cs}, we therefore subtract from each $SWR_{cs-biased}$ time series the SWR-forcing from anomalies of τ_{dust}, following the methodology of Evan and Mukhopadhyay (2010). Since the NCEP SWR_{cs} does not include radiative forcing from dust, no correction is applied before calculating the clear-sky bias based on NCEP. The difference between each of the three "true" clear-sky estimates and $SWR_{cs-biased}$, which includes dust-accumulation biases, then gives three estimates of the time-dependent dust-accumulation bias at each location ($B_{cs-NCEP}$, $B_{cs-MERRA}$, and $B_{cs-buoy}$). Note that positive values of $B_{cs-NCEP}$, $B_{cs-MERRA}$, and $B_{cs-buoy}$ represent an attenuation of buoy SWR due to dust accumulation. Note also that $B_{cs-NCEP}$ likely represents an upper bound on the magnitude of the clear-sky dust-accumulation bias at a given location because the NCEP SWR_{cs} time series do not include forcing from dust aerosols.

The advantages of the clear-sky method over the rain-free and swap methods are that the clear-sky method does not rely on the ISCCP-FD SWR climatology, which contains time-dependent biases, and it provides a continous record of the dust accumulation bias. The downside of the clear-sky method is that it relies on accurate time series of buoy clear-sky SWR and the “true” clear-sky SWR. In an effort to quantify the uncertainties associated with the “clear-sky” method we have considered three independent estimates of SWR_{cs}.

4 Results

In this section, we first present a qualitative analysis of dust-accumulation biases using data from the mooring at 12°N, 38°W, which experiences a high annual mean τ_{dust} and strong seasonal variability (Fig. 6a). The dust-accumulation bias index and time-dependent biases at each PIRATA mooring location are then quantified using the methods described in the previous section.

4.1 Time series at 12°N, 38°W

Examples of dust-accumulation biases at the 12°N, 38°W location are shown in Fig. 6b. During the middle of 2003 a large bias (defined as the daily ISCCP-FD SWR climatology minus the daily maximum buoy SWR) is evident in the PIRATA SWR record. The bias increased from 10–20 W m^{-2} in February–March 2003 to 50–75 W m^{-2} in June–July. The bias increased most rapidly during the period in boreal spring and summer with the highest τ_{dust} and no significant rainfall, defined here as >5 mm day^{-1}. After the mooring was serviced in July 2003 and the old radiometer was replaced with a new one, the bias decreased by about 100 W m^{-2}, from 50 W m^{-2} before the sensor replacement to -50 W m^{-2} immediately after the replacement (Fig. 6b). Note that a negative bias does not imply that accumulated dust enhances the buoy SWR, because of the way the bias is defined.

Similar biases developed at 12°N, 38°W during 2005 and 2006, though they were noticeably smaller in magnitude compared to the bias in 2003 (Fig. 6b). During July 2005 there was a jump up in buoy SWR of ∼50 W m^{-2} when a new sensor was installed. The bias reached a maximum more than a month before the sensor swap and then decreased slightly as rainfall began, suggesting that rainfall may have partially rinsed the radiometer. Further evidence of rinsing can be found during boreal summer and fall of 2006 at the same location. The maximum bias of 2006 was ∼50 W m^{-2} and occurred in June. Between July and September the bias gradually decreased as precipitation became more frequent and more intense. Between September and December there was no obvious bias in buoy SWR, suggesting that rainfall completely rinsed the radiometer. September–December is also the time of year when τ_{dust} is low and dust is therefore less likely to accumulate on the sensor. As a result, when the sensor was swapped in December 2006, there was not a noticable jump up in SWR, in contrast to the pronounced jumps during 2003 and 2005.

In summary, there is compelling evidence of significant (greater than 50 W m^{-2}) dust-accumulation biases in the SWR record at 12°N, 38°W, one of the locations with highest annual mean τ_{dust}. There is also evidence of strong interannual variability in the dust bias that is likely due to a combination of variability in τ_{dust}, timing of sensor swaps, and rinsing of the sensor by rainfall.

4.2 Dust-accumulation bias index

In agreement with the qualitative analysis at 12°N, 38°W, the dust-accumulation indices from the rain-free and swap methods tend to be largest between 8°N–20°N (Fig. 7). This is the region where the annual mean τ_{dust} is highest and where the seasonal cycle of τ_{dust} is generally out of phase with that of rainfall (i.e., rainfall is low in boreal spring and summer, when τ_{dust} is high). The rain-free index reaches 50 W m^{-2} at

12°N, 23°W, where annual mean τ_{dust} is >0.4 and rainfall is low ($\sim$5 cm mo^{-1}) and confined to the boreal fall. The much weaker index at 21°N, 23°W is surprising, given the high τ_{dust} and very low rainfall. The low value at this location may due to dust falling off the sensor between deployments. The significant bias at 8°N, 38°W is also surprising, given the high annual mean rainfall. At this location, τ_{dust} is highest in boreal winter and spring, and the dust layer is lower in the atmosphere (e.g., Yu et al. 2010), possibly explaining the stronger than expected bias at this location. Despite large rain-free dust-accumulation indices at 12°N and 21°N along 23°W, these values are not statistically significant because of the small sample size (record lengths of 2–5 years; Fig. 2). Along 38°W, the dust-accumulation indices calculated using the "swap" method are similar to the indices calculated using the "rain-free" method. Only the statistical significance of each swap bias index is therefore shown in Fig. 7. Swap bias indices could not be calculated at the 12°N and 21°N moorings along 23°W because of shorter records.

In contrast to the bias indices at locations in the tropical North Atlantic, the PIRATA moorings at 0° and 10°W along the equator have much lower values despite annual mean values of τ_{dust} that are comparable to those along 38°W (Fig. 7). The weaker biases at the equatorial locations result from an in-phase relationship between τ_{dust} and rainfall: the highest τ_{dust} occurs in boreal winter and spring (e.g., Husar et al. 1997), when there is abundant rainfall to rinse the SWR sensors. Biases are weak and insignificant at the other equatorial locations and at most of the locations in the tropical South Atlantic. The exception is at 19°S, 34°W, where there are rain-free and swap indices of 15 W m^{-2} and 18 W m^{-2}, respectively, despite very low τ_{dust} (<0.05 in the annual mean). It is therefore unlikely that the biases at this location are caused by dust buildup. Instead, there may be a seasonally-dependent bias in the ISCCP-FD SWR climatology that explains the bias. With the exception of the 0°, 0° location, everywhere a rain-free index was computed it is positive (i.e., buoy SWR decreases in time relative to ISCCP-FD SWR climatology), consistent with the sensor drift biases described in Section 3.

We tested the sensitivity of the rain-free and swap indices to the choice of rainfall criterion, using values from 2–20 mm day^{-1}, and the choice of the averaging period (10–45 days) and found that the results are not significantly changed. In the rest of this section we focus on the locations where the rain-free index is statistically significant (8°N–15°N along 38°W).

4.3 Time-dependent biases

Here the mean seasonal cycles and longer timescale variability of dust-accumulation biases are shown for the high-dust locations in the central tropical North Atlantic (8°N–15°N along 38°W). At each location, the mean seasonal cycle of the dust bias and its relationship with the seasonal cycles of τ_{dust} and rainfall are discussed first, followed by a discussion of longer timescale variability.

The mean seasonal cycles and interannual-decadal variability of the dust-accumulation biases at 15°N, 12°N, and 8°N along 38°W, are shown in Figs. 8-13. At 15°N, the rain-free and swap biases (B_{rain}, B_{swap}, respectively) and the buoy and NCEP clear-sky biases ($B_{cs-buoy}$ and $B_{cs-NCEP}$, respectively) all show a pronounced maximum of 30 to 35 W m^{-2} in July. The maximum of the MERRA clear-sky bias ($B_{cs-MERRA}$) also occurs in July, but is 15–20 W m^{-2} smaller in comparison. The individual swap biases (red circles and squares in Fig. 8a) give a mean of 40 W m^{-2} in July, which is consistent with B_{rain}, B_{swap}, $B_{cs-buoy}$, and $B_{cs-NCEP}$. We therefore hypothesize that the lower values of $B_{cs-MERRA}$ relative to the other dust-accumulation bias estimates may be due to biases in the MERRA clear-sky climatology.

July is the month with the largest mean τ_{dust} and is the transition period between the dry season (January–June) and the rainy season (August–October) (Fig. 8b,c). Dust accumulates most rapidly on the sensor during May–July, when τ_{dust} >0.3 and rainfall is very light. The arrival of heavy rain in August quickly rinses the SWR sensor, evident in the rapid decrease in dust-accumulation bias during that month (Fig. 8a). During February–March there is a weaker maximum in the dust-accumulation bias that is most pronounced in B_{swap} and $B_{cs-buoy}$. However, there is less consistency in the magnitude of this secondary maximum between the different bias estimates.

In Fig. 8a, the mean of the individual swap biases (B_i; red circles and squares) generally does not equal the mean of the continuous time-dependent swap biases (B_c; B_{swap} is the mean seasonal cycle of B_c and is given by the red line in Fig. 8a). This inequality occurs because each B_c is calculated by extending a B_i value backward in time (see section 3). There are therefore generally a larger number of B_c values for a given calendar month than B_i values. The difference between the mean of B_c and the mean of B_i is especially apparent during March–April, when each B_i is larger than the mean of the B_c values. The difference between the means may be due to biases in the ISCCP-FD SWR climatology. It is also possible that the dust-accumulation biases during March–April happened to be larger in the years when B_i values were available compared to the years when B_i values were not available.

During April 2002 the swap bias calculated from the recovered sensor (B_{lab}; filled red square in Fig. 8a) agrees reasonably well with the corresponding B_i (filled red circle in Fig. 5a). B_{lab} is about 10 W m^{-2} smaller than B_i, possibly because some of the dust fell off the sensor during its transit from the field to the laboratory or was washed off by sea-spray during the recovery of the sensor from the mooring. In contrast, in July 2003 B_{lab} is about 35 W m^{-2} smaller than the corresponding B_i (filled red square and circle, respectively, in Fig. 8a). The discrepancy is due in large part to a time-dependent drift in the sensor output that ranged from zero at the beginning of the deployment to -7.4% at the end of the deployment (Freitag and Brown, manuscript in preparation). This sensor drift was erroneously interpreted as a dust-accumulation bias in B_i. Caution must therefore be used when interpreting a bias during a single deployment. However, a more extensive analysis of the drift bias, based on 316 calibration pairs, found a mean of 1.5% of the incident radiation and a standard deviation of 2.4% (Freitag and Brown, manusrcipt in prep.). Assuming a mean SWR value of 240 W m^{-2}, the dust-accumulation biases in the high-dust region (8°N–20°N) are on average 4–10 times as large as the corresponding drift biases.

In addition to a strong seasonal cycle of the dust-accumulation bias, there is noticeable interannual variability (Fig. 9a). Comparison of the buoy SWR anomalies (without any bias correction) to the dust-accumulation bias estimates shows that most of the mean bias with respect to ISCCP-FD SWR and low-frequency (i.e., period >1 year) variability of the buoy SWR can be attributed to the dust-accumulation bias (Fig. 9b). There is a pronounced upward trend in buoy SWR between 1998 and 2005 that is likely spurious, caused by a decreasing trend in the dust-accumulation bias (Fig. 9b, Table 1). Anomalous decreases in buoy SWR during 2002–03 and 2007 are also likely due to large dust buildup during those years. The decreasing trend in the dust-accumulation bias during 1998–2005 is consistent with a decreasing trend in τ_{dust} during the same period (e.g., Evan et al. 2008, Foltz and McPhaden 2008). After removal of the dust accumulation bias from the buoy SWR, the upward trend is significantly reduced and the buoy SWR anomalies show better agreement with anomalies of cloud forcing (Fig. 9c and Table 1). The mean buoy SWR increases by 8–16 W m^{-2}, and the interannual standard deviation decreases by about 50% (Table 1). An upward trend in buoy SWR of 8–14 W m^{-2} per decade remains after removal of the dust-accumulation bias (Table 1). The trend may be caused by a concurrent decrease in τ_{dust} (and associated attenuation of SWR) or a decrease in cloudiness, though such an analysis is beyond the scope of this paper.

At 12°N, 38°W, most of the bias estimates show a maximum of 20 to 40 W m^{-2} during June–July, consistent with the seasonal cycle of dust-accumulation bias at 15°N, 38°W (Fig. 10). In contrast, there is a pronounced maximum in $B_{cs-buoy}$ of 35 W m^{-2} in early April, followed by smaller values (10 to 20 W m^{-2}) during June–July. The smaller values of $B_{cs-buoy}$ during late May through early July compared to the other bias estimates may be due to persistent dust buildup on the sensor and a lack of sensor swaps at this time of year, the combination of which would generate a high bias in the buoy SWR_{cs} estimates. This reasoning may also explain why during May–June $B_{cs-buoy}$ at 15°N, 38°W is smaller than most of the other bias estimates at this location (Fig. 8a). Year-to-year variations of the different dust-accumulation bias estimates are generally consistent and are in agreement with the results at 15°N (Fig. 11 and Table 1).

At 8°N, 38°W the seasonal cycle of τ_{dust} peaks in March–April, 3–4 months earlier than at 12°N and 15°N, and the dry season at 8°N lasts only from February–April (Fig. 12). As a result, there is less time for dust to accumulate on the sensor at 8°N, and the maximum seasonal bias is slightly weaker at 8°N compared to the other locations.

There are significant differences between the interannual variability at 8°N and at 12°N and 15°N (Fig. 13a). Most notably, the bias at 8°N is weak during 2007, but at 15°N it is the strongest on record using most methodologies. The discrepancies are likely due to differences in the seasonality of dust deposition and rainfall. Consistent with the results at 12°N and 15°N, most of the interannual–decadal variability and long-term trend of the buoy SWR at 8°N can be explained by the dust accumulation bias (Fig. 13b and Table 1). Removal of the bias from the buoy SWR record improves the SWR-cloud anomaly correlation dramatically, from -0.2 to -0.6 (Fig. 13c and Table 1).

5 Summary and Discussion

We have shown that the SWR measurements from several PIRATA moorings in the tropical North Atlantic (8°N–21°N) are biased low due to dust buildup on the SWR sensors. At a given location in the tropical North Atlantic, the magnitude of the bias tends to increase in time until either the dusty sensor is swapped for a clean one or significant rainfall rinses the sensor. The timing of the sensor swaps, generally about once per year in March–April or July–August, and the commencement of the rainy season in June–July, results in periods of 2–4 months during boreal winter–spring and spring–summer when dust can accumulate on the SWR sensor.

To determine which PIRATA SWR records are likely to be affected by dust-accumulation biases, a simple dust bias index was created that represents the maximum bias at each location, averaged over all deployments. Statistically significant values of this index of 21 to 27 W m^{-2} (indicating an attenuation of SWR due to accumulated dust) were found at 8°N, 12°N, and 15°N along 38°W. These are the PIRATA locations with long time series of SWR (>11 years) and where the annual mean τ_{dust} is high

($\sim$0.3). Large values were also found at 21°N, 23°W and 12°N, 23°W (20 W m^{-2} and 50 W m^{-2}, respectively), though these values are not statistically significant because of much shorter time series. The largest value at 12°N, 23°W is consistent with the highest annual mean τ_{dust} of 0.5 at this location.

Daily time series of the dust-accumulation bias at three locations along 38°W were computed using three methods. Significant annual mean biases and strong seasonal and interannual variability of the dust-accumulation bias were found at all locations. Annual mean biases range from 10 W m^{-2} to 20 W m^{-2}. Peak-to-peak seasonal amplitudes of the bias at these locations are typically 30 W m^{-2}, and interannual standard deviations are 3–4 W m^{-2}. There are also noticeable negative linear trends in the magnitude of the accumulation bias at 8°N, 38°W and 15°N, 38°W. Removal of the dust-accumulation bias from SWR records of the 38°W moorings significantly improves the correlation between anomalies of buoy SWR and satellite cloud cover.

Three different methods for quantifying the time-dependent dust-accumulation biases were developed, each with certain strengths and weaknesses. Overall, the methods give similar results, though differences can be large between some methods at a given location. It is concluded that the MERRA clear-sky method is likely to give the most accurate bias at most locations, and we therefore recommend using this method to correct the PIRATA SWR time series for dust-accumulation biases if a single method is desired. We note, however, that the MERRA clear-sky method likely underestimates the true dust-accumulation bias at 15°N, 38°W. Time series of SWR from the high-dust locations (8°N, 12°N, and 15°N along 38°W; and 12°N and 21°N along 23°W), corrected using the MERRA clear-sky method, are accessible from PMEL's PIRATA web site.

These results have important implications for the use of SWR data from PIRATA moorings in the high-dust region of the tropical North Atlantic. Overall, the SWR data during September–January do not appear to be affected significantly by dust-accumulation biases since this is the time of year when there is significant rainfall to rinse the SWR sensors. For most applications, the data during these months can likely be used without a bias correction. During February–October the biases are much larger and exhibit strong interannual variability. These data should therefore be corrected for dust-accumulation biases and then used with caution in scientific analyses.

It is possible that the SWR biases documented in this study may be useful for quantifying dust deposition in the tropical North Atlantic. Deposition rates have been estimated from satellite τ_{dust} and dust transport models, but there are no long observational records of dust deposition over the tropical Atlantic Ocean. As a result, there are large uncertainties in the dust deposition rate and its seasonal, interannual, and longer timescale variability. One way to validate the deposition rates inferred from the PIRATA dust-accumulation biases would be to quantify the mass of dust on each sensor when it is swapped each year and then compare to the deposition inferred from the accumulation bias. Even with such a validation, deposition rates inferred from the results presented here would likely be a lower bound on the true deposition rate since an unknown amount of dust falls off each sensor during its ∼one-year deployment. Quantification of dust deposition from aerosol samplers (e.g., Sholkovitz and Sedwick 2006) moored at the same locations as the PIRATA buoys would provide more accurate time series of deposition into the future and could be used to reconstruct dust deposition from the accumulation biases going back to 1998.

Acknowledgments

The authors thank Rick Lumpkin, Renellys Perez, and three anonymous reviewers for helpful suggestions. Funding was provided by NOAA/CPO grant NA10OAR4310136 and base funds from NOAA/AOML. This publication is partially funded by the Joint Institute for the Study of the Atmosphere and Ocean (JISAO) under NOAA Cooperative Agreement No. NA17RJ1232 and NA10OAR4320148, contribution #2063. This is PMEL contribution #3874.

References

Bonjean, F., and G. S. E. Lagerloef (2002), Diagnostic model and analysis of the surface currents in the tropical Pacific Ocean, *J. Phys. Oceanogr.*, *32*, 2938–2954.

Bourlès, B., and Coauthors, 2008: The PIRATA program: History, accomplishments, and future directions. *Bull. Am. Meteorol. Soc.*, **89**, 1111–1125.

Evan, A. T., A. K. Heidinger, and M. J. Pavolonis, 2006: Development of a new over-water advanced very high resolution radiometer dust detection algorithm. *Int. J. Remote Sens.*, **27**, 3903–3924.

Evan, A. T., A. K. Heidinger, R. Bennartz, V. Bennington, N. M. Mahowald, H. Corrada-Bravo, C. S. Velden, G. Myhre, and J. P. Kossin, 2008: Ocean temperature forcing by aerosols across the Atlantic tropical cyclone development region. *Geochem. Geophys. Geosyst.*, **9**, Q05V04, doi:10.1029/ 2007GC001774.

Evan, A. T., and S. Mukhopadhyay, 2010: African Dust over the Northern Tropical Atlantic: 1955–2008. *J. Appl. Meteorol. Clim.*, **49**, 2213–2229.

Foltz, G. R., and M. J. McPhaden, 2005: Mixed layer heat balance on intraseasonal time scales in the northwestern tropical Atlantic Ocean. *J. Climate*, **18**, 4168–4184.

Foltz, G. R., and M. J. McPhaden, 2006: Unusually warm sea surface temperatures in the tropical North Atlantic during 2005. *Geophys. Res. Lett.*, **33**, L19703, doi:10.1029/2006GL027394.

Foltz, G. R., and M. J. McPhaden, 2008: Trends in Saharan dust and tropical Atlantic climate during 1980-2006. *Geophys. Res. Lett.*, **35**, L20706, doi:10.1029/2008GL035042.

Freitag, H. P., Y. Feng, L. J. Mangum, M. J. McPhaden, J. Neander, and L. D.

Stratton, 1994: Calibration procedures and instrumental accuracy estimates of TAO temperature, relative humidity and radiation measurements, *NOAA TM ERL PMEL-104*, 32 pp., Natl. Oceanic and Atmos. Admin., Silver Spring, Md., 1994.

Gao, Y., and Coauthors, 2001: Seasonal distributions of aeolian iron fluxes to the global ocean. *Geophys. Res. Lett.*, **28**, 29–32.

Ginoux, P., and Coauthors, 2001: Sources and distributions of dust aerosols simulated with the GOCART model. *J. Geophys. Res.*, **106**, 20,255–20,274.

Husar, R., J. Prospero, and L. Store, 1997: Characterization of tropospheric aerosols over the oceans with the NOAA advanced very high resolution radiometer optical thickness operational product. *J. Geophys. Res.*, **102**, 16,889–16,909.

Ignatov, A., and L. L. Stowe, 2002: Aerosol retrievals from individual AVHRR channels, Part I: Retrieval algorithm and transition from Dave to 6S Radiative Transfer Model. *J. Atmos. Sci.*, **59**, 313–334.

Kalnay, E., and Coauthors., 1996: The NCEP/NCAR 40-year reanalysis project. *Bull. Am. Meteorol. Soc.*, **77**, 437–471.

Kaufman, Y. J., I. Koren, L. A. Remer, D. Tanr, P. Ginoux, and S. Fan, 2005: Dust transport and deposition observed from the Terra-Moderate Resolution Imaging Spectroradiometer (MODIS) spacecraft over the Atlantic Ocean. *J. Geophys. Res.*, **110**, D10S12, doi:10.1029/2003JD004436.

Kumar, B. P., J. Vialard, M. Lengaigne, V. S. N. Murty, and M. J. McPhaden, 2012: TropFlux: Air-sea fluxes for the global tropical oceans–Description and evaluation. *Climate Dyn.*, **38**, 1521–1543, doi:10.1007/s00382-011-1115-0.

MacWhorter, M. A., and R. A. Weller, 1991: Error in measurements of incoming shortwave radiation made from ships and buoys. *J. Atmos. Ocean. Tech.*, **8**, 108–117.

McPhaden, M. J., A. J. Busalacchi, R. Cheney, J. R. Donguy, K. S. Gage, D. Halpern, M. Ji, P. Julian, G. Meyers, G. T. Mitchum, P. P. Niiler, J. Picaut, R. W. Reynolds, N. Smith, K. Takeuchi, 1998: The Tropical Ocean-Global Atmosphere (TOGA) observing system: A decade of progress. *J. Geophys. Res.*, **103**, 14,169–14,240.

McPhaden, M. J., G. Meyers, K. Ando, Y. Masumoto, V. S. N. Murty, M. Ravichandran, F. Syamsudin, J. Vialard, L. Yu, and W. Yu, 2009: RAMA: The Research Moored Array for African-Asian-Australian Monsoon Analysis and Prediction. *Bull. Am. Meteorol. Soc.*, **90**, 459–480.

Medovaya, M., D. E. Waliser, R. A. Weller, and M. J. McPhaden, 2002: Assessing ocean buoy shortwave observations using clear-sky model calculations. *J. Geophys. Res.*, **107**, 3014, doi:10.1029/2000JC000558.

Moulin, C., and I. Chiapello, 2004: Evidence of the control of summer atmospheric transport of African dust over the Atlantic by Sahel sources from TOMS satellites (1979 2000). *Geophys. Res. Lett.*, **31**, L02107, doi:10.1029/2003GL018931.

Moyer, K. A., and R. A. Weller, 1997: Observations of surface forcing from the Subduction Experiment: A comparison with global model products and climatological datasets. *J. Climate*, **10**, 2725–2742.

Pinker, R. T., H. M. Wang, and S. A. Grodsky, 2009: How good are ocean buoy observations of radiative fluxes? *Geophys. Res. Lett.*, **36**, L10811, doi:10.1029/2009GL037840.

Prospero, J. M., and T. N. Carlson, 1972: Vertical and areal distribution of Saharan dust over the western equatorial North Atlantic Ocean. *J. Geophys. Res.*, **77**, 5255–5265.

Prospero, J. M., P. Ginoux, O. Torres, S. E. Nicholson, and T. E. Gill, 2002: Environmental characterization of global sources of atmospheric soil dust identified with the NIMBUS 7 Total Ozone Mapping Spectrometer (TOMS) absorbing aerosol product. *Rev. Geophys.*, **40**, 1002, doi:10.1029/2000RG000095.

Remer, L. A., and Coauthors, 2005: The MODIS aerosol algorithm, products, and validation. *J. Atmos. Sci.*, **62**, 947–973.

Rienecker, M. M., M. J. Suarez, R. Gelaro, R. Todling, J. Bacmeister, E. Liu, M. G. Bosilovich, S. D. Schubert, L. Takacs, G.-K. Kim, S. Bloom, J. Chen, D. Collins, A. Conaty, A. da Silva, et al., 2011. MERRA - NASA's Modern-Era Retrospective Analysis for Research and Applications. *J. Climate*, **24**, 3624–3648, doi: 10.1175/JCLI-D-11-00015.1.

Rossow, W. B., and R. A. Schiffer (1991), ISCCP cloud data products, *Bull. Am. Meteorol. Soc.*, *72*, 2–20.

Serra, Y. L., and M. J. McPhaden, 2003: Multiple time- and space-scale comparisons of ATLAS buoy rain gauge measurements with TRMM satellite precipitation measurements. *J. Appl. Meteorol.*, **42**, 1045–1059.

Sholkovitz, E. R., and P. N. Sedwick, 2006: Open-ocean deployment of a buoy-mounted aerosol sampler on the Bermuda Testbed Mooring: Aerosol iron and sea salt over the Sargasso Sea. *Deep-Sea Res. I*, **53**, 547–560, doi:10.1016/j.dsr.2005.12.002.

Sun B. M., L. S. Yu, and R. A. Weller, 2003: Comparisons of surface meteorology and turbulent heat fluxes over the Atlantic: NWP model analyses versus moored buoy. *J. Climate*, **16**, 679–695.

Waliser, D. E., R. A. Weller, and R. D. Cess, 1999: Comparisons between buoy-observed, satellite-derived, and modeled surface shortwave flux over the subtropical North Atlantic during the Subduction Experiment. *J. Geophys. Res.*, **104**, 31,301–31,320.

Yu, H., M. Chin, D. M. Winker, A. H. Omar, Z. Liu, C. Kittaka, and T. Diehl, 2010: Global view of aerosol vertical distributions from CALIPSO lidar measurements and GOCART simulations: Regional and seasonal variations. *J. Geophys. Res.*, **115**, D00H30, doi:10.1029/2009JD013364.

Zhang, Y., W. B. Rossow, A. A. Lacis, V. Oinas, and M. I. Mishchenko, 2004: Calculation of radiative fluxes from the surface to top of atmosphere based on ISCCP and other global data sets: Refinements of the radiative transfer model and the input data. *J. Geophys. Res.*, **109**, D19105, doi:10.1029/2003JD004457.

Zhu, A., V. Ramanathan, F. Li, and D. Kim, 2007: Dust plumes over the Pacific, Indian, and Atlantic oceans: Climatology and radiative impact. *J. Geophys. Res.*, **112**, D16208, doi:10.1029/2007JD008427.

Table 1 Statistics of daily SWR records from the 15°N, 12°N, and 8°N PIRATA moorings along 38°W. First column represents the uncorrected SWR time series and the second, third, and fourth columns are the time series after removal of the buoy, NCEP, and MERRA clear-sky dust accumulation biases, respectively. Reliable statistics could not be generated from the rain-free and swap bias-corrected time series because of significant gaps in the bias time series. First row for each location is the correlation of the mooring SWR anomaly (with respect to ISCCP-FD seasonal cycle) with anomalies of $(1 - e^{-\tau_{cloud}})$. Second row is the record-length mean SWR in W m^{-2}. Third row is the record-length linear trend in SWR in W m^{-2} per decade. Smaller values in columns 2–4 compared to column 1 indicate that the upward linear trends in the corrected times series are smaller than in the uncorrected time series. Fourth row is the standard deviation of the SWR anomaly time series in W m^{-2}. Before calculating the correlation (first row) and standard deviation (last row) the SWR and $(1 - e^{-\tau_{cloud}})$ time series were smoothed with consecutive passes of 181-day and 259-day running mean filters.

	Uncorr.	Buoy	NCEP	MERRA
15°N, 38°W				
Corr(SWR,Cloud)	-0.54	-0.62	-0.66	-0.65
Mean SWR	231	247	246	239
Trend SWR	14.8	7.9	11.5	14.0
Std. SWR	7.3	2.7	2.8	3.7
12°N, 38°W				
Corr(SWR,Cloud)	-0.63	-0.78	-0.81	-0.88
Mean SWR	222	235	242	234
Trend SWR	4.5	2.6	3.5	4.4
Std. SWR	9.8	7.1	5.7	6.1
8°N, 38°W				
Corr(SWR,Cloud)	-0.19	-0.60	-0.67	-0.64
Mean SWR	211	222	228	223
Trend SWR	13.7	3.1	1.0	4.2
Std. SWR	9.8	5.7	5.3	5.1

Figure Captions

Fig. 1 Annual mean surface shortwave radiation (SWR) from ISCCP-FD during 1984–2009 (shaded) and dust aerosol optical depth (τ_{dust}) from MODIS during 2003–2010 (contoured every 0.1 units). Black squares and circles indicate locations of PIRATA moorings and the length of the SWR time series at each location in data-years (i.e., total record length minus gaps).

Fig. 2 Availability of daily SWR data from each PIRATA mooring.

Fig. 3 Daily anomalies (with respect to the ISCCP-FD seasonal cycle) of PIRATA SWR as a function of anomalous cloud forcing, expressed as the fraction of incoming solar radiation that is attenuated by clouds, at (a) 15°N, 38°W, (b) 12°N, 38°W, and (c) 8°N, 38°W. SWR and cloud forcing time series at each location have been filtered to removed variability with periods >120 days. Red lines are third-order polynomial fits to the data.

Fig. 4 Daily anomalies (with respect to the ISCCP-FD seasonal cycle) of SWR from the high-dust PIRATA moorings, excluding 21°N, 23°W, as a function of (a) the time-integral of τ_{dust} and (b) τ_{dust}. The starting time for the integral is the most recent day with significant rainfall or the most recent sensor swap date, whichever occurred most recently. The red line in (a) is a nonlinear fit based on (5).

Fig. 5 (a) Mean seasonal cycle of clear-sky SWR at the 12°N, 38°W PIRATA mooring location calculated from the mooring SWR time series (black), and from the NCEP/NCAR (red) and MERRA reanalyses. (b) Sensitivity of the mooring clear-sky SWR to the length of the SWR time series, based on a 20-sample permutation test. Record lengths range from three years (black) to 11 years (purple). (c) Standard deviation corresponding to each curve in (b). All time series have been smoothed with a 31-day running mean filter.

Fig. 6 Daily mean time series at the 12°N, 38°W PIRATA mooring location during 2003 and 2005–2006. (a) SWR attenuation due to suspended dust, expressed as a percentage of the incoming SWR. (b) SWR measured by the mooring (black); climatological SWR from monthly ISCCP-FD, averaged during 1998–2010 (blue); days with rainfall >5 mm (red stars, plotted according to the buoy SWR value on that day), and SWR sensor swap dates (vertical green lines). (c) Rainfall measured by the mooring. Red line represents 5 mm d^{-1}. In (a), SWR attenuation is shown instead of τ_{dust} in order to de-emphasize very large values of τ_{dust}.

Fig. 7 Annual mean τ_{dust} (shaded) and TRMM rainfall (contours, cm mo^{-1}). White circles show the dust accumulation bias index, based on the rain-free method, at the PIRATA locations where it could be calculated. Filled white circles indicate where the rain-free index is significantly different than zero at the 5% level. Black dots indicate where the index, calculated using the swap method, is significant at the 5% level. White x's mark the locations where the bias could not be calculated.

Fig. 8 Daily mean seasonal cycles at 15°N, 38°W. (a) The dust accumulation bias based on the rain-free (black curve), swap (red curve), and clear-sky (blue, green, and purple curves for the buoy, NCEP, and MERRA clear-sky values, respectively) methods. Grey and blue shading indicate one standard error of the rain-free and buoy clear-sky estimates, respectively. Red circles are the individual swap biases. Filled red squares are biases based on laboratory comparisons between the retrieved dusty sensor and a clean sensor, and filled red circles are the corresponding swap biases. (b) τ_{dust} (black line) with one standard error shown as grey shading. (c) Same as (b) except rainfall from the mooring. Each time series has been smoothed with consecutive passes of 21-day and 29-day running mean filters.

Fig. 9 Daily time series at 15°N, 38°W during 1998–2011. (a) Dust accumulation bias calculated using the swap method when available and the rain-free method otherwise (black), and using the buoy (blue), NCEP (green), and MERRA (pink) clear-sky methods. (b) Anomalies (with respect to ISCCP-FD mean seasonal cycle) of the mooring SWR (red) and accumulation biases shown in (a). Cloud forcing anomaly (red) and SWR anomaly from the mooring after subtraction of the buoy clear-sky bias (black). Time series in (a) have been smoothed with a 31-day running mean filter. Each time series in (b) and (c) has been smoothed with consecutive passes of 181-day and 259-day running mean filters to emphasize interannual variability.

Fig. 10 Same as Fig. 8 except for the 12°N, 38°W PIRATA location. The gap in the rain-free time series in (a) during August–November is the result of persistent rainfall during that period.

Fig. 11 Same as Fig. 9 except for the 12°N, 38°W PIRATA location.

Fig. 12 Same as Fig. 8 except for the 8°N, 38°W PIRATA location.

Fig. 13 Same as Fig. 9 except for the 8°N, 38°W PIRATA location.

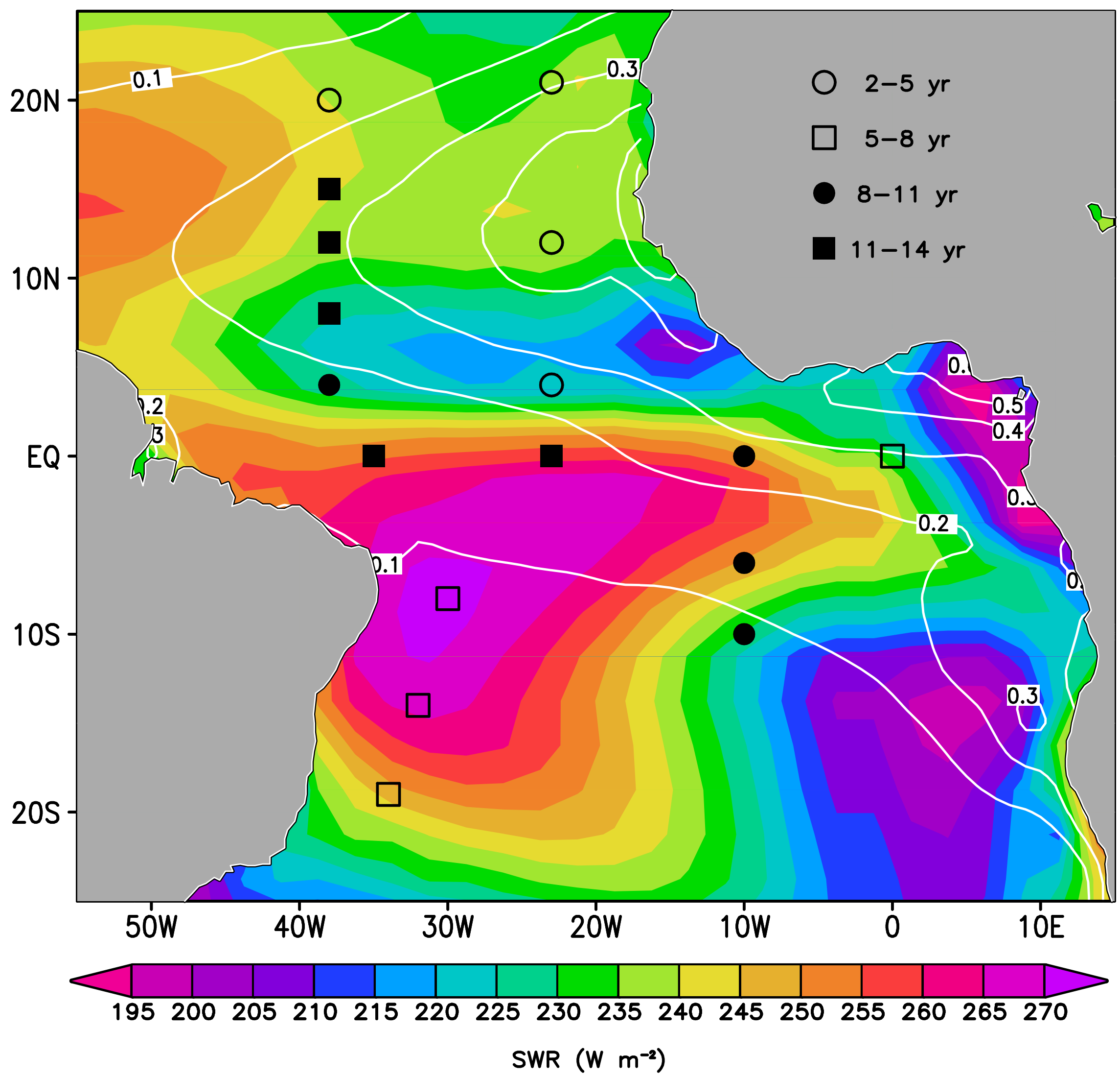

Fig. 1 Annual mean surface shortwave radiation (SWR) from ISCCP-FD during 1984–2009 (shaded) and dust aerosol optical depth (τ_{dust}) from MODIS during 2003–2010 (contoured every 0.1 units). Black squares and circles indicate locations of PIRATA moorings and the length of the SWR time series at each location in data-years (i.e., total record length minus gaps).

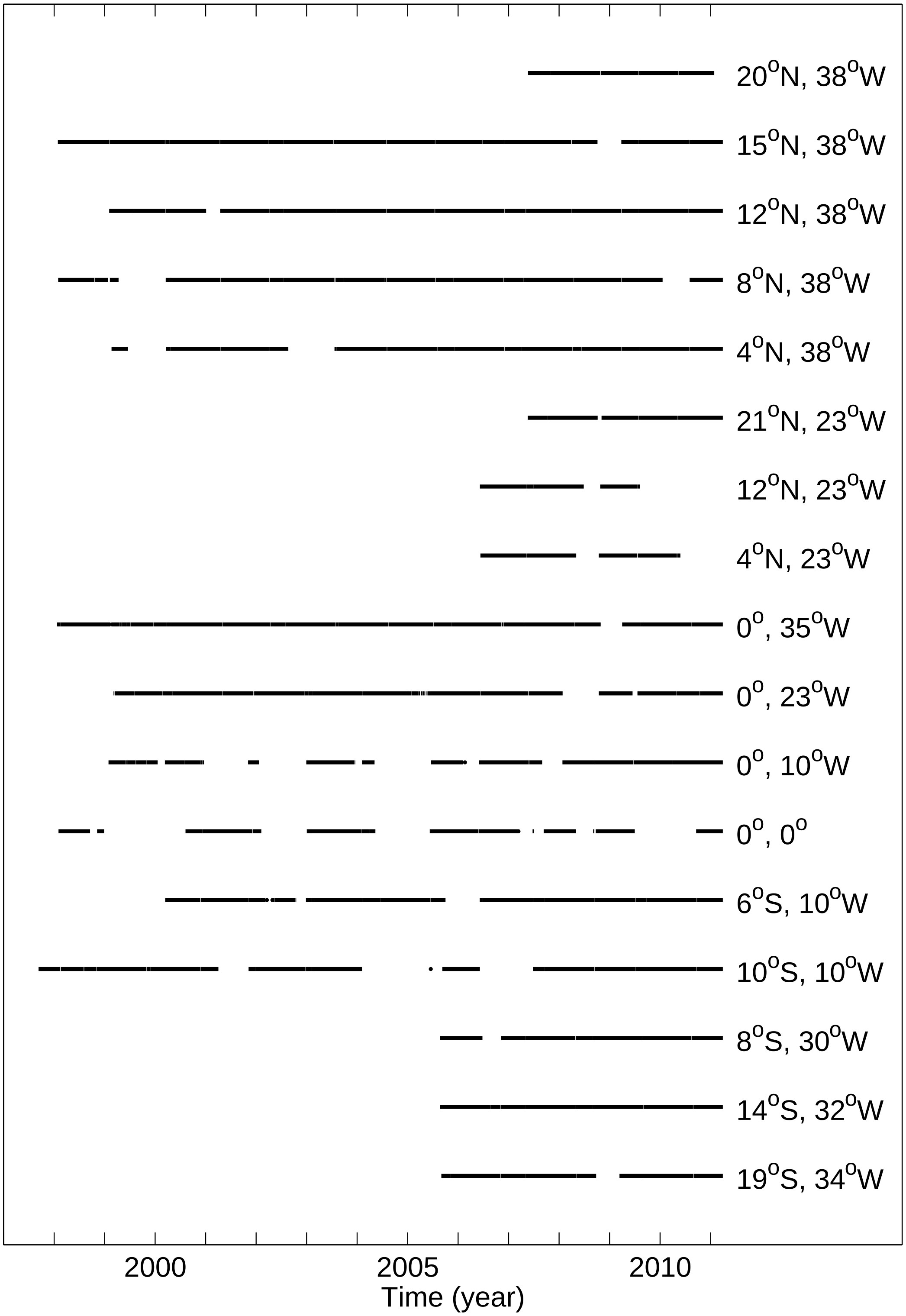

Fig. 2 Availability of daily SWR data from each PIRATA mooring.

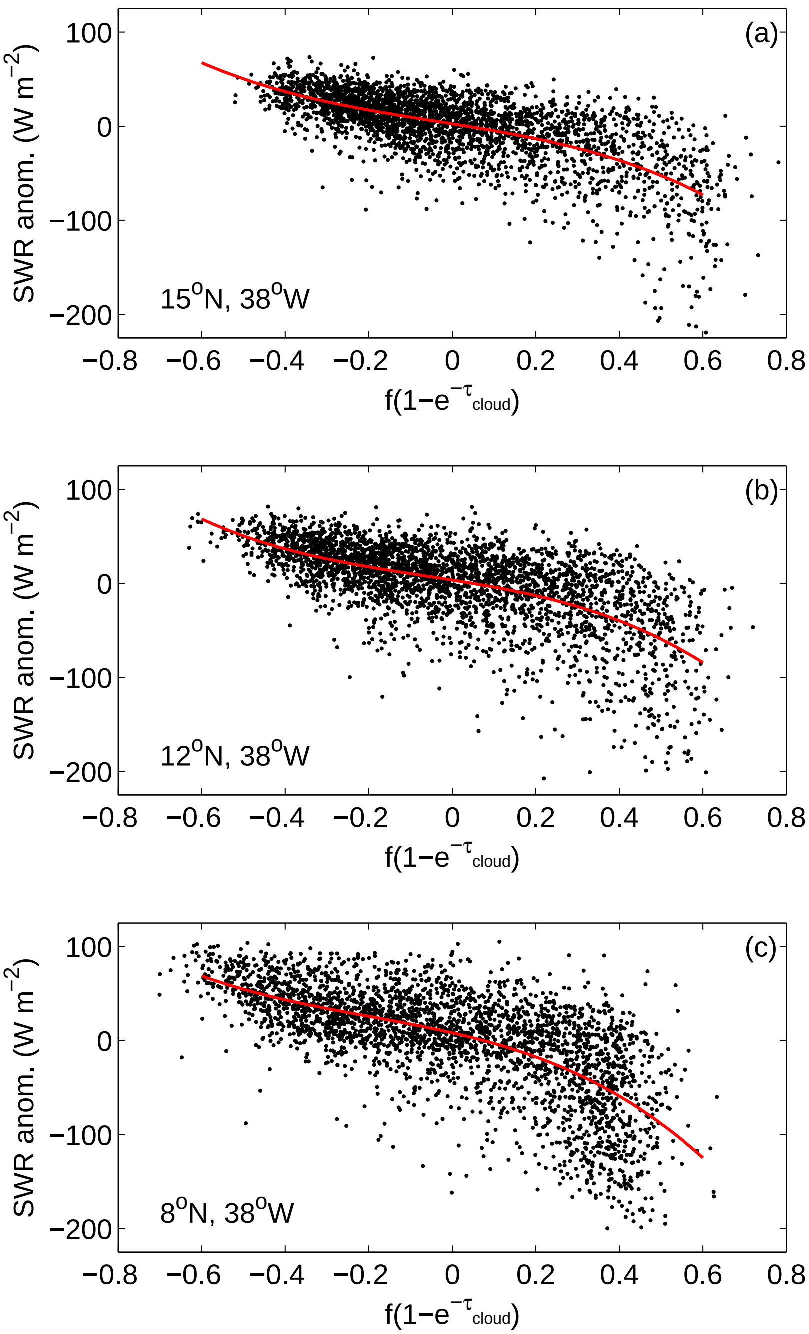

Fig. 3 Daily anomalies (with respect to the ISCCP-FD seasonal cycle) of PIRATA SWR as a function of anomalous cloud forcing, expressed as the fraction of incoming solar radiation that is attenuated by clouds, at (a) 15°N, 38°W, (b) 12°N, 38°W, and (c) 8°N, 38°W. SWR and cloud forcing time series at each location have been filtered to removed variability with periods >120 days. Red lines are third-order polynomial fits to the data.

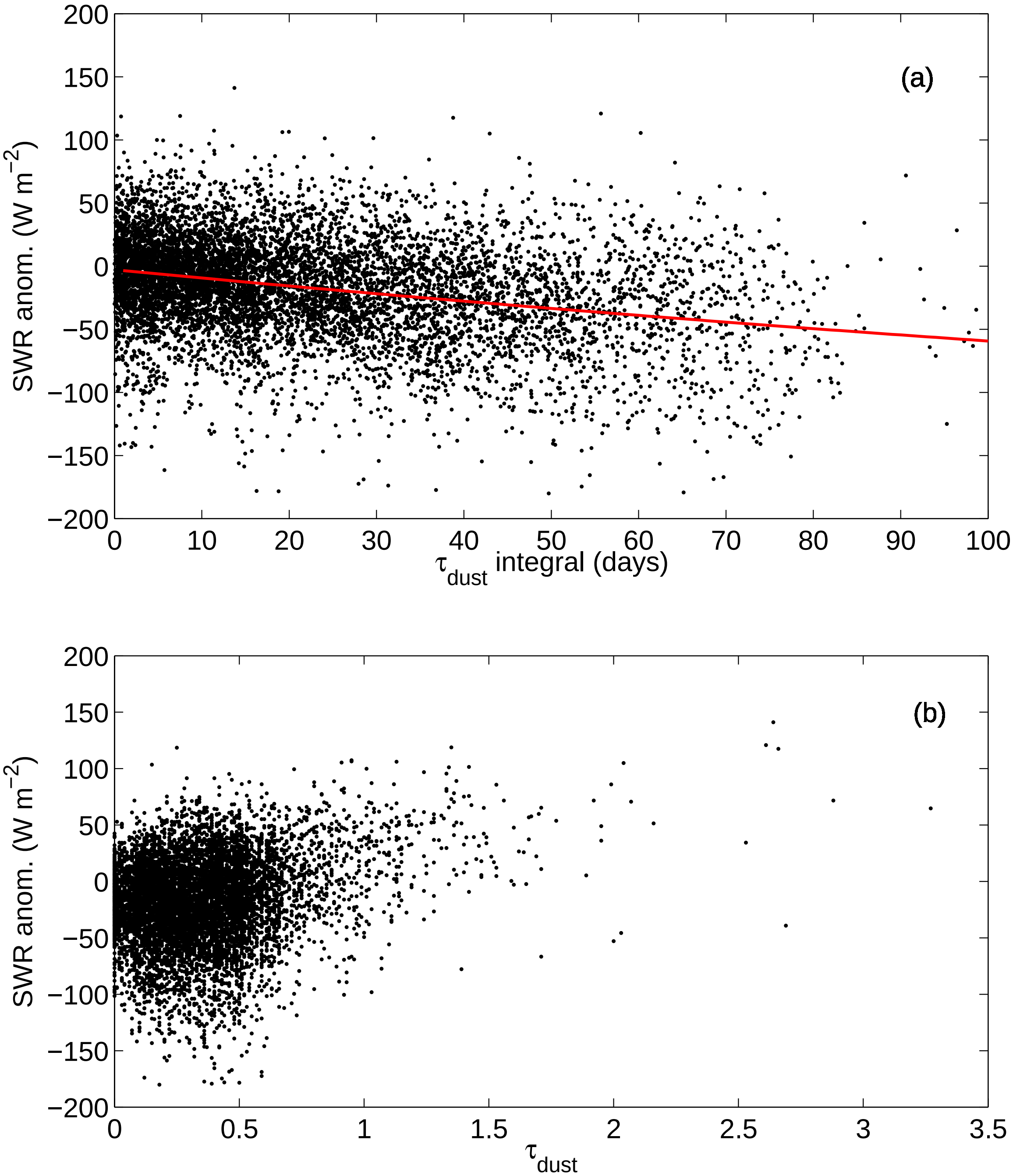

Fig. 4 Daily anomalies (with respect to the ISCCP-FD seasonal cycle) of SWR from the high-dust PIRATA moorings, excluding 21°N, 23°W, as a function of (a) the time-integral of τ_{dust} and (b) τ_{dust}. The starting time for the integral is the most recent day with significant rainfall or the most recent sensor swap date, whichever occurred most recently. The red line in (a) is a nonlinear fit based on (5).

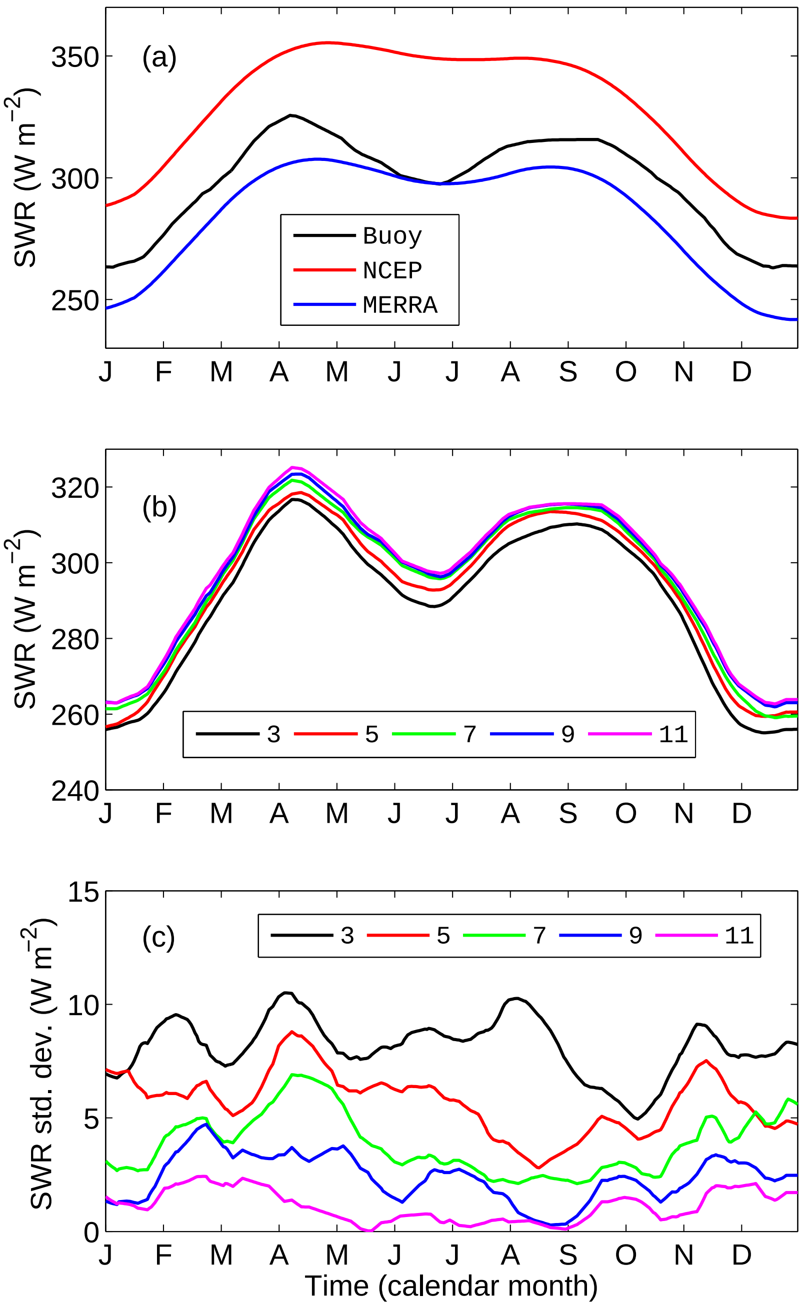

Fig. 5 (a) Mean seasonal cycle of clear-sky SWR at the 12°N, 38°W PIRATA mooring location calculated from the mooring SWR time series (black), and from the NCEP/NCAR (red) and MERRA reanalyses. (b) Sensitivity of the mooring clear-sky SWR to the length of the SWR time series, based on a 20-sample permutation test. Record lengths range from three years (black) to 11 years (purple). (c) Standard deviation corresponding to each curve in (b). All time series have been smoothed with a 31-day running mean filter.

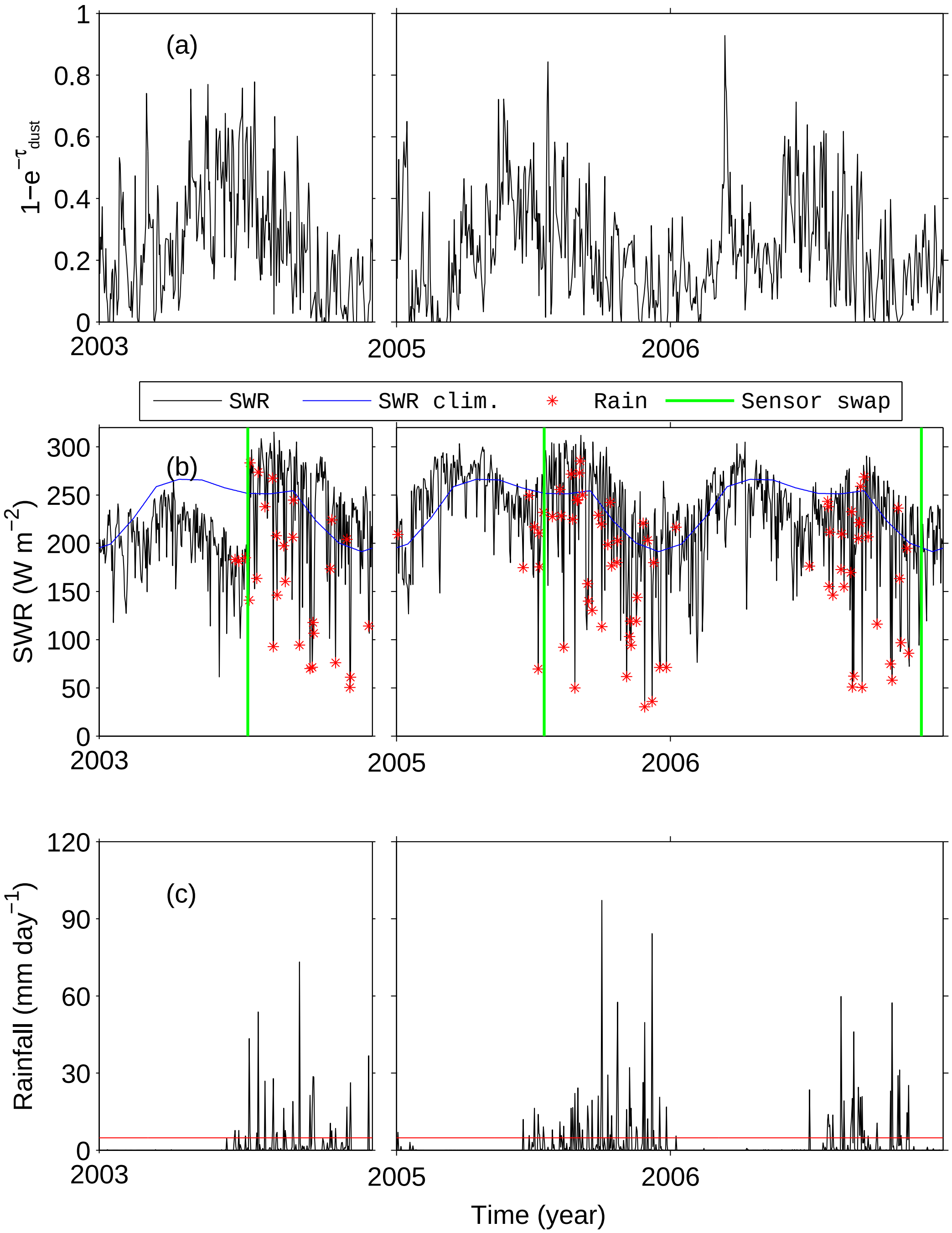

Fig. 6 Daily mean time series at the 12°N, 38°W PIRATA mooring location during 2003 and 2005–2006. (a) SWR attenuation due to suspended dust, expressed as a percentage of the incoming SWR. (b) SWR measured by the mooring (black); climatological SWR from monthly ISCCP-FD, averaged during 1998–2010 (blue); days with rainfall >5 mm (red stars, plotted according to the buoy SWR value on that day), and SWR sensor swap dates (vertical green lines). (c) Rainfall measured by the mooring. Red line represents 5 mm d^{-1}. In (a), SWR attenuation is shown instead of τ_{dust} in order to de-emphasize very large values of τ_{dust}.

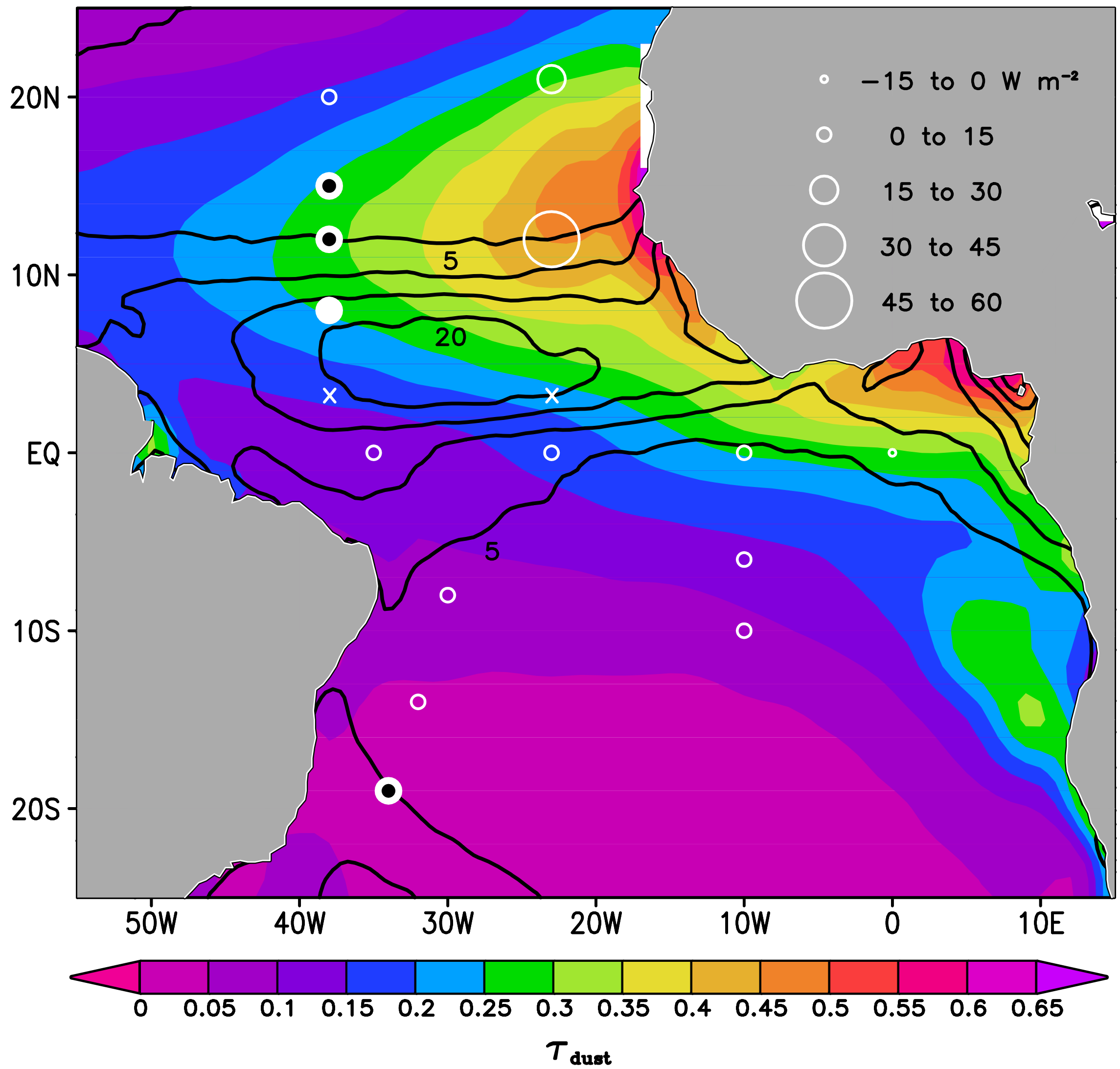

Fig. 7 Annual mean τ_{dust} (shaded) and TRMM rainfall (contours, cm mo^{-1}). White circles show the dust accumulation bias index, based on the rain-free method, at the PIRATA locations where it could be calculated. Filled white circles indicate where the rain-free index is significantly different than zero at the 5% level. Black dots indicate where the index, calculated using the swap method, is significant at the 5% level. White x's mark the locations where the bias could not be calculated.

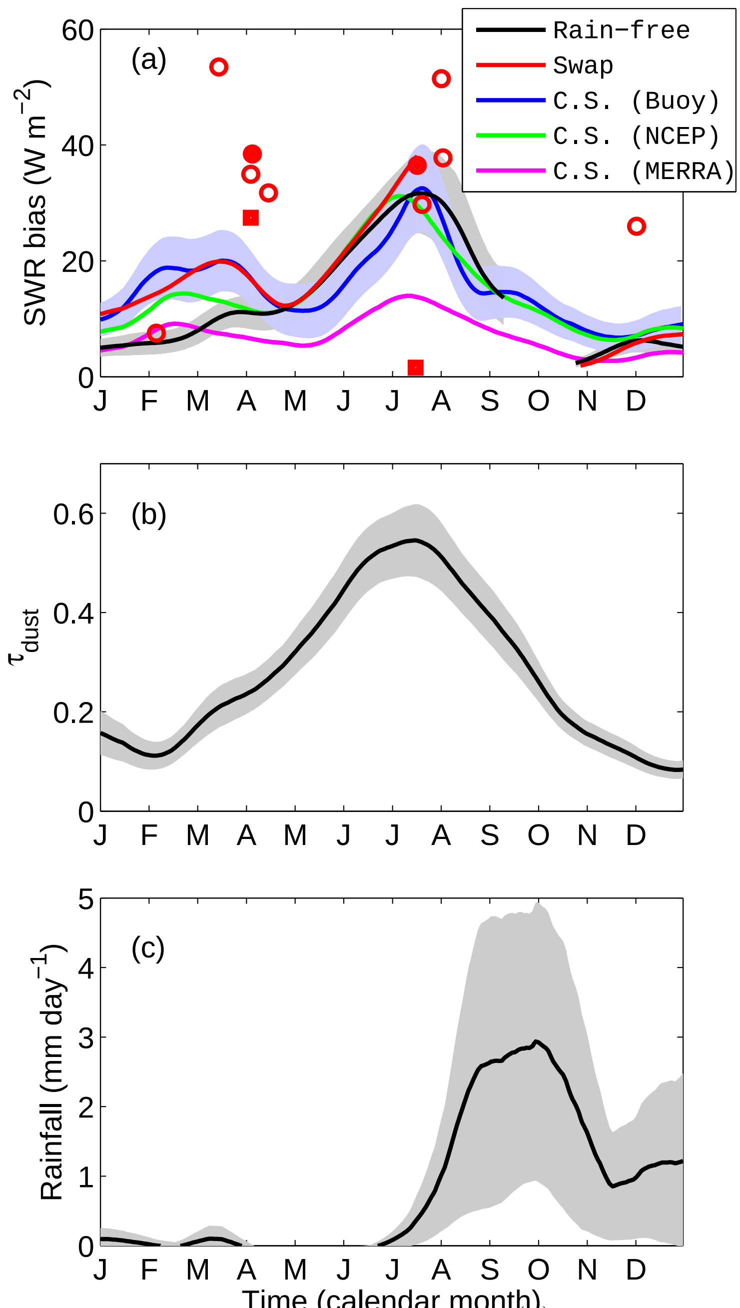

Fig. 8 Daily mean seasonal cycles at 15°N, 38°W. (a) The dust accumulation bias based on the rain-free (black curve), swap (red curve), and clear-sky (blue, green, and purple curves for the buoy, NCEP, and MERRA clear-sky values, respectively) methods. Grey and blue shading indicate one standard error of the rain-free and buoy clear-sky estimates, respectively. Red circles are the individual swap biases. Filled red squares are biases based on laboratory comparisons between the retrieved dusty sensor and a clean sensor, and filled red circles are the corresponding swap biases. (b) τ_{dust} (black line) with one standard error shown as grey shading. (c) Same as (b) except rainfall from the mooring. Each time series has been smoothed with consecutive passes of 21-day and 29-day running mean filters.

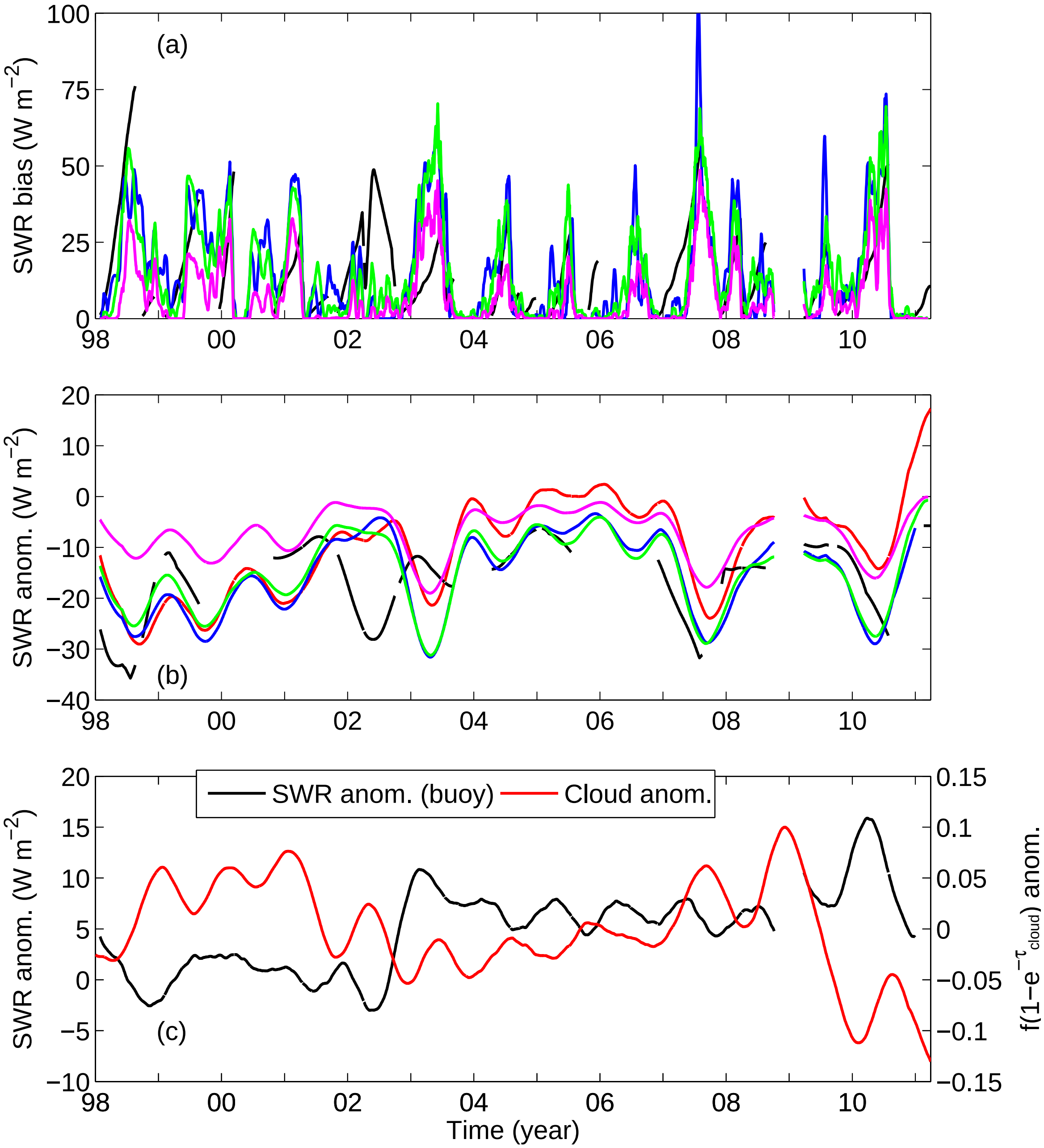

Fig. 9 Daily time series at 15°N, 38°W during 1998–2011. (a) Dust accumulation bias calculated using the swap method when available and the rain-free method otherwise (black), and using the buoy (blue), NCEP (green), and MERRA (pink) clear-sky methods. (b) Anomalies (with respect to ISCCP-FD mean seasonal cycle) of the mooring SWR (red) and accumulation biases shown in (a). Cloud forcing anomaly (red) and SWR anomaly from the mooring after subtraction of the buoy clear-sky bias (black). Time series in (a) have been smoothed with a 31-day running mean filter. Time series in (b) and (c) have been smoothed with consecutive passes of 181-day and 259-day running mean filters to emphasize interannual variability.

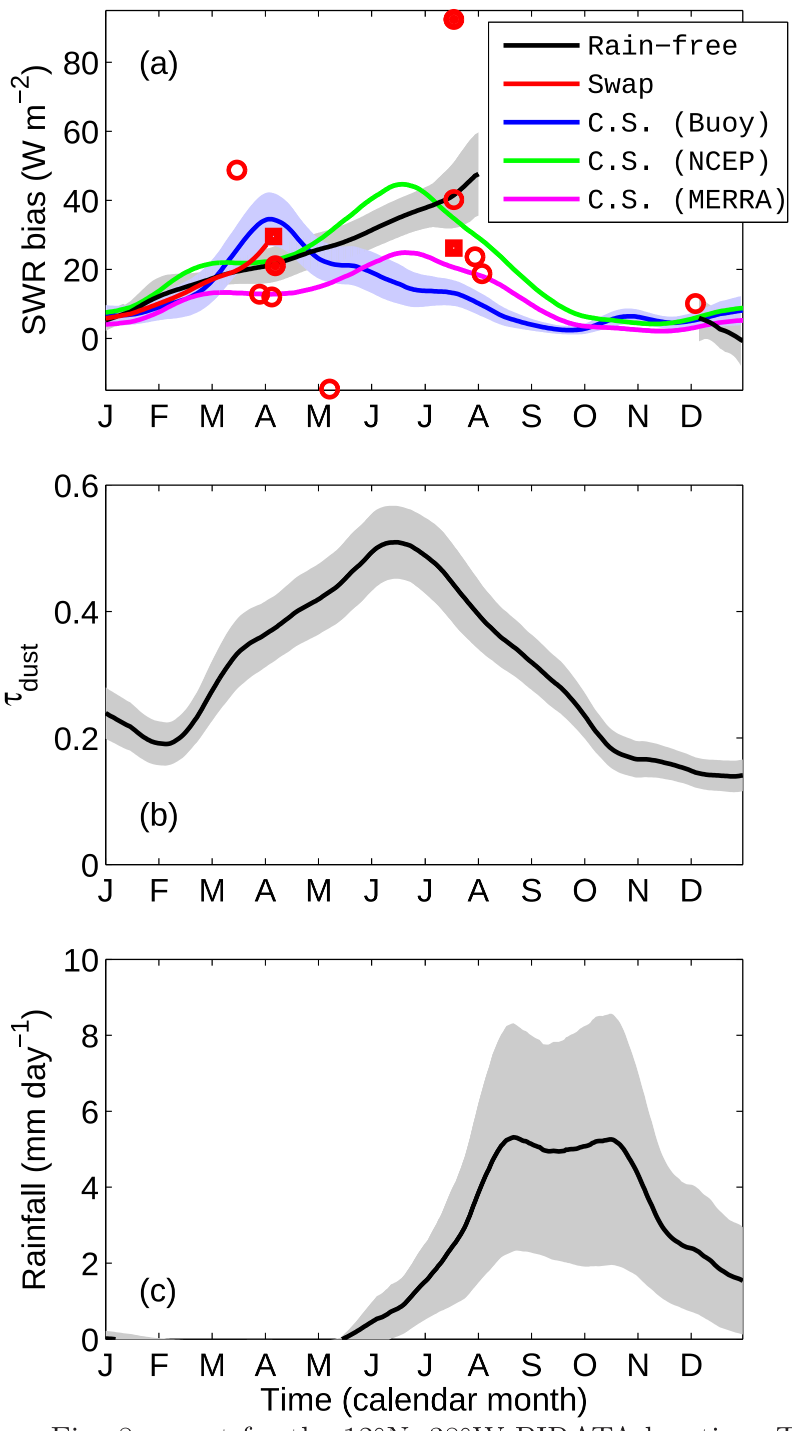

Fig. 10 Same as Fig. 8 except for the 12°N, 38°W PIRATA location. The gap in the rain-free time series in (a) during August–November is the result of persistent rainfall during that period.

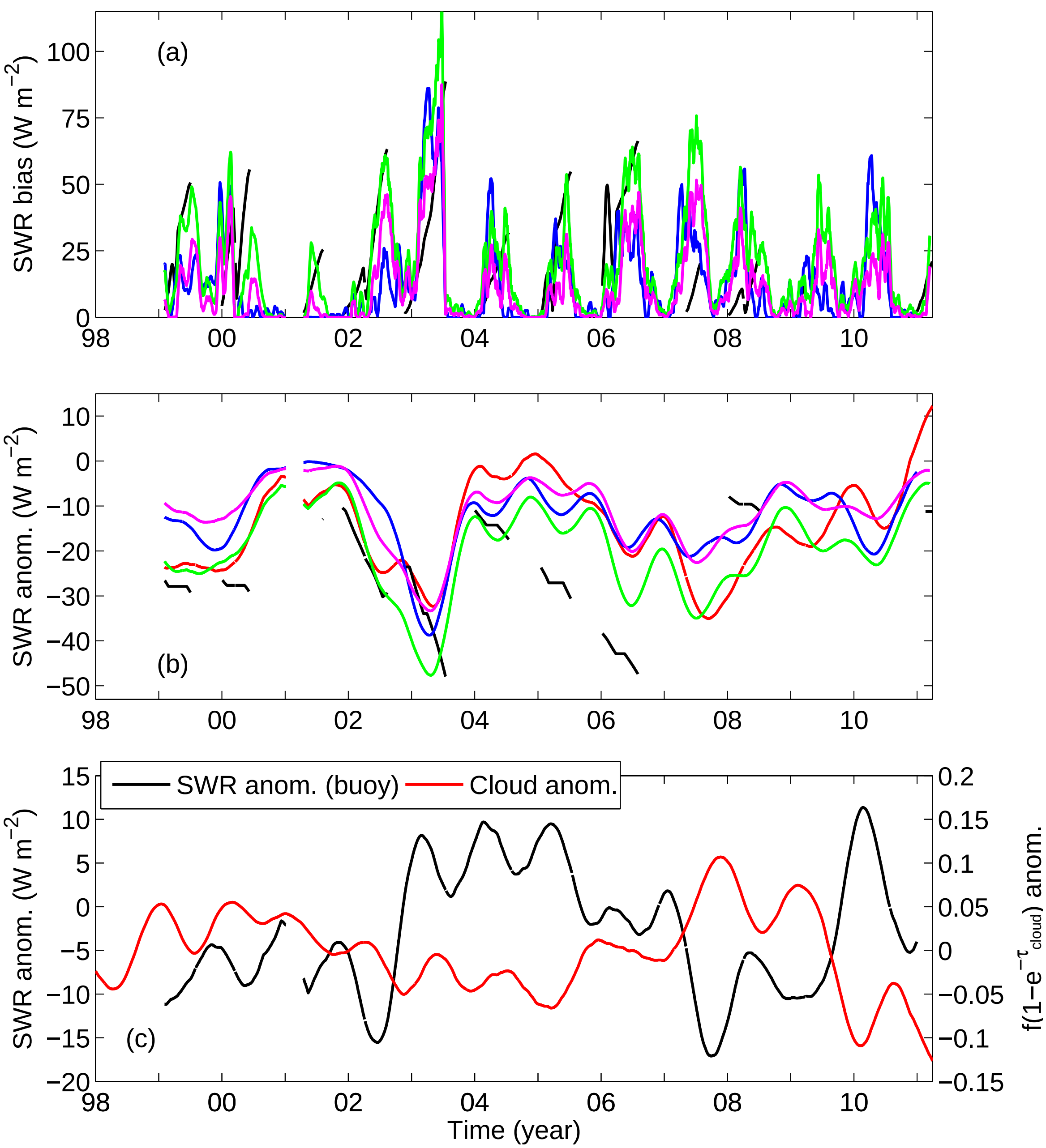

Fig. 11 Same as Fig. 9 except for the 12°N, 38°W PIRATA location.

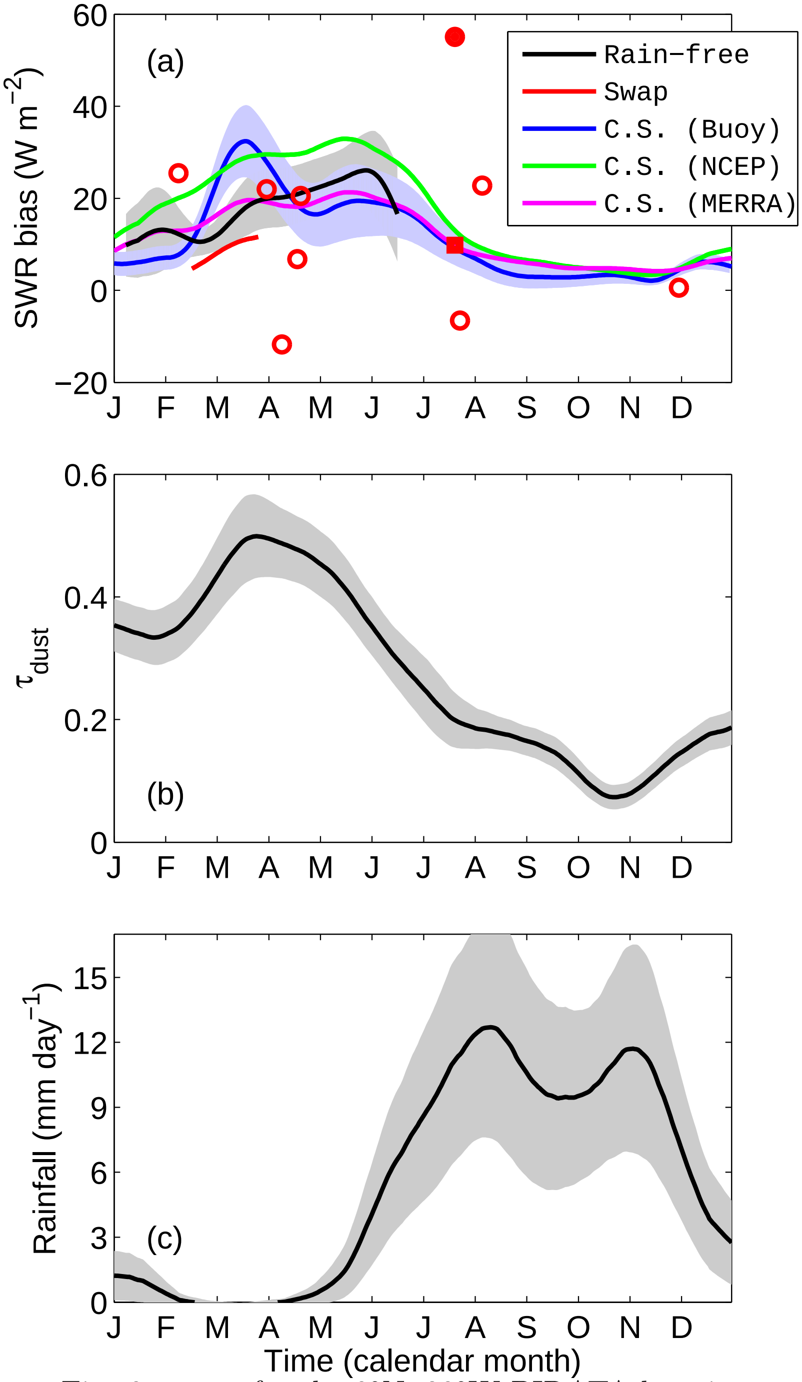

Fig. 12 Same as Fig. 8 except for the 8°N, 38°W PIRATA location.

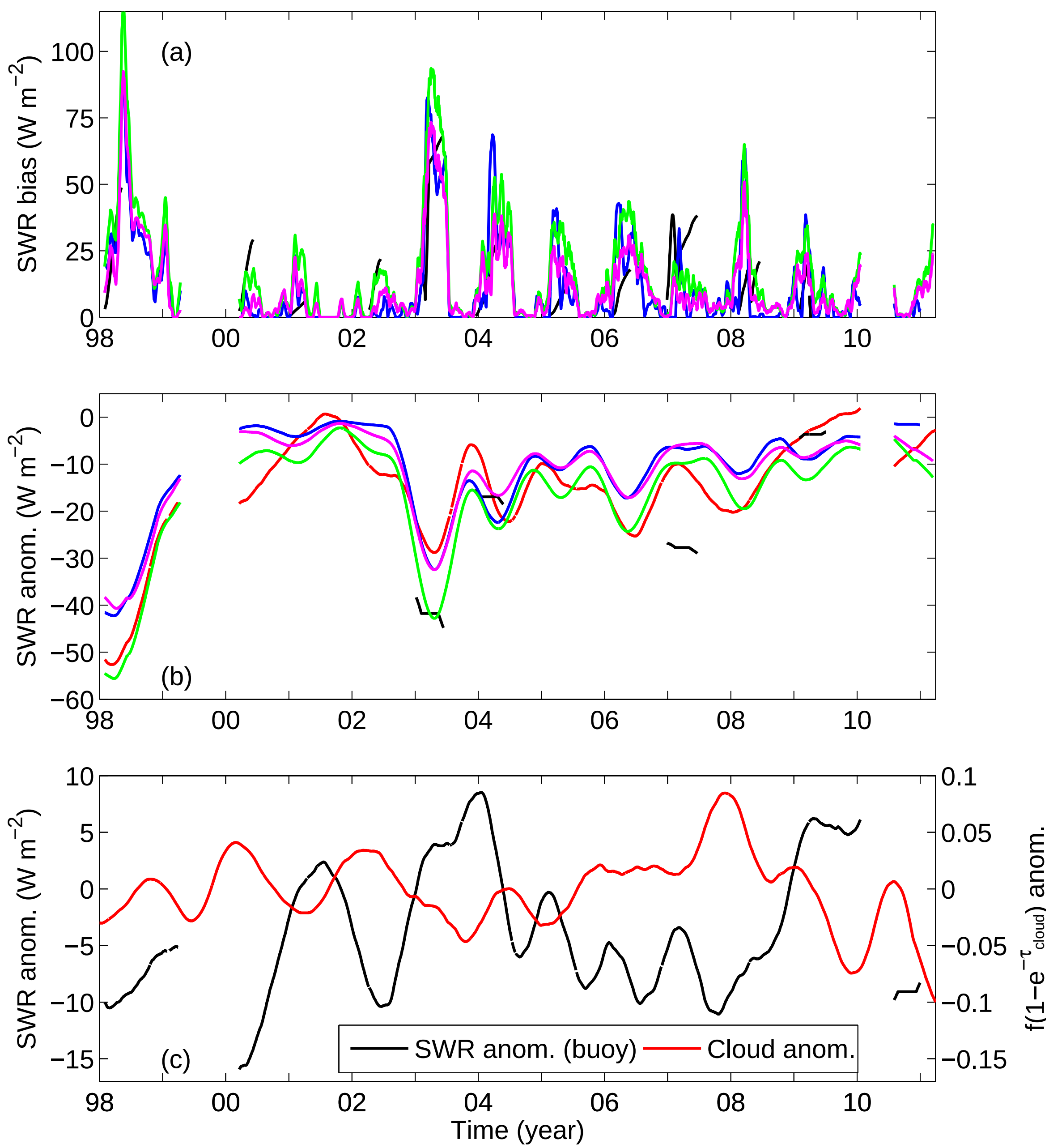

Fig. 13 Same as Fig. 9 except for the 8°N, 38°W PIRATA location.